



Flux Calibration of the COS G160M Grating at Lifetime Position 6

Lauren P. Miller¹, Ravi Sankrit¹, William J. Fischer¹, Elaine Frazer¹, Nick Indriolo^{1,2},
Christian I. Johnson¹, and Nathaniel E.B. Kerman^{1,3}

¹ Space Telescope Science Institute, Baltimore, MD

²AURA for European Space Agency, STScI, USA

³ Laboratory for Atmospheric and Space Physics, Boulder, CO

25 September 2024

ABSTRACT

We report on the creation and validation of the photometric throughput table (FLUXTAB) and flat-field file (FLATFILE) for the sixth lifetime position (LP6) of the Cosmic Origins Spectrograph (COS) Far Ultraviolet (FUV) detector, which became active in October 2022 at the beginning of Cycle 30. Using observations of the flux-standard star WD0308-565, we derive new sensitivity curves and low-order flat fields (L-FLATS) at LP6 for both segments of the G160M central wavelengths. The L-FLATS and sensitivity curves for LP6 agree within 2% of those at LP4, the previous LP of the G160M cenwaves. In addition, the LP6 FLUXTAB and FLATFILE reference files meet our absolute and relative flux calibration requirements of less than 5% and 2%, respectively.

Contents

1. Introduction	2
2. Program Design and Observations	3
3. Analysis	3

4. Scientific Validation of the Flux Calibration	6
5. Reference Files Delivered and Conclusion	7
Change History for COS ISR 2023-16	7
References	9
Appendix	25

1. Introduction

The Cosmic Origins Spectrograph (COS) far-ultraviolet (FUV) detector uses a windowless micro-channel plate (MCP) with two segments, FUVA and FUVB. Over time, repetitive and prolonged light exposure leads to a decline in the number of electrons per incident photon, called “gain sag”. To mitigate the effect of gain sag and extend the usable lifespan of COS, the Y-position of the science spectrum for a given aperture, central wavelength, and grating is periodically shifted to a more pristine region of the detector. Each location is known as a lifetime position (LP) and is measured as an offset from LP1 (Fischer et al. 2022). The most recent lifetime position move was to LP6 in October 2022 at the beginning of Cycle 30, which placed the G160M grating (central wavelengths 1533 to 1623 angstroms) at +6.5 arcseconds from LP1 (James et al. 2023a, James et al. 2023b, Sankrit et al. 2023).

A new photometric throughput table (FLUXTAB) and flat-field file (FLATFILE) are required with each lifetime position change to maintain the absolute and relative flux calibration accuracy for COS (<5 % and <2 %, respectively). The FLATFILE is an L-FLAT image, which the CalCOS pipeline uses to remove the low spatial frequency variations in the detector. These changes scale to about 1/20 of the extent of the detector and are larger in the dispersion direction. The L-FLAT is a one-dimensional curve that is replicated to form a two-dimensional image and is a function of XCORR. The FLATFILE consists of a primary header and two 16384×1024 IMAGE extensions, one for each detector segment. It also corrects for grid wire shadows and an effect of small-scale geometric distortion. The FLUXTAB provides the information needed to convert from corrected detector counts to flux units for each segment, optical element, aperture, and central wavelength. These files contain arrays of wavelengths and sensitivities which can be interpolated onto the observed wavelength grid. The net counts can then be divided by the sensitivity curves to produce flux-calibrated spectra.

Additional reference files have to be created to account for updated spectral extraction and wavelength calibration (see Section 3), as well as new gain maps (GSAGTAB) and a new bad pixel table (BPIXTAB). A summary of the calibration efforts for LP6 can be found in Sankrit et al. 2023.

This ISR describes our process for deriving the sensitivities and flat fields at LP6. Section 2 outlines our program design and associated observations used in the flux calibration. Section 3 reviews our methodology for constructing the sensitivity curves and flat fields and how we technically validated our results by comparing them to the existing LP4 FLUXTAB and FLATFILE reference files. In Section 4, we test that our

Table 1. Observations Used in Creation of FLUXTAB and FLATFILE (PID 16906, WD0308-565, FUV A and FUV B)

Obs. Mode	Obs. Date	Vist No.	FP-POS=1	FP-POS=2	FP-POS=3	FP-POS=4
G160M/1533	2022-04-18	01	letb01agq	letb01b8q	letb01beq	letb01brq
G160M/1577	2022-04-16	02	letb02flq	letb02ftq	letb02g0q	letb02g6q
G160M/1589	2022-04-19	03	letb03g8q	letb03geq	letb03goq	letb03gwq
G160M/1600	2022-04-20	04	letb04mwq	letb04n2q	letb04neq	letb05r2q
G160M/1611	2022-04-21	05	letb05r2q	letb05r8q	-	-
G160M/1611	2022-05-14	55	-	-	letb55onq	letb55owq
G160M/1623	2022-04-22	06	letb06umq	letb06usq	letb06v4q	letb06vaq

new files meet our absolute and relative flux calibration standards, and finally, in Section 5, we present our conclusions and list the reference files we delivered.

2. Program Design and Observations

To create the new LP6 FLUXTAB and FLATFILE, we made use of HST/COS FUV A and FUV B G160M data taken during eleven orbits across seven visits of the white dwarf HST flux-standard star WD0308-565. This target is a HST flux standard star used several times in the past to calibrate COS observing modes. These visits (01, 02, 03, 04, 05, 06, and 55) covered central wavelengths 1533, 1577, 1589, 1600, 1611, and 1623 angstroms under the program ‘‘COS FUV LP6 Calibration: Profiles, Traces, Sensitivities, Flat Fields and Spatial Resolution’’ (PID:16906; PI: E. Frazer). The exposure times of the observations, taken at all four FP-POS settings in April and May 2022, were selected to achieve the required signal-to-noise (S/N) of 50 per resolution element. To minimize the effects of time-dependent sensitivity (TDS) on the flux calibration, all visits were planned within a four-week time window and close to the connection visits in the program ‘‘Cycle 29 COS FUV Spectroscopic Sensitivity Monitor’’ (PID:16830; PI: K. Rowlands). A partial failure at FP-POS 3 and 4 occurred in visit 05, and replacement data was obtained in visit 55. Table 1 lists the data used in the analysis, where the entries are the root names of the files containing the data for each cenwave and FP-POS.

3. Analysis

For each COS FUV mode, the net count rate registered by the detector, C , in units of counts s^{-1} pixel $^{-1}$, depends on the wavelength (λ) and the position (X) along the detector’s dispersion direction and is assumed to be a product of the source flux, sensitivity, and flat fields. This relationship can be expressed as,

$$C(\lambda, X) = F(\lambda) \times S(\lambda) \times L(X) \times P(X) \quad (1)$$

where $F(\lambda)$ is the source flux density ($\text{erg s}^{-1} \text{cm}^{-2} \text{\AA}^{-1}$) and $S(\lambda)$ is the detector sensitivity ($\text{count s}^{-1} \text{pixel}^{-1} / \text{erg s}^{-1} \text{cm}^{-2} \text{\AA}^{-1}$). The remaining terms describe the dimensionless flat fields, where $L(X)$ is the L-FLAT or low spatial frequency flat field, and $P(X)$ is the P-FLAT or the pixel-to-pixel high variation across the detector. As such, the flux calibration can be separated into a flat field that accounts solely for the detector response and a sensitivity function that accounts for the wavelength-dependent attenuation due to optical effects.

We can utilize Equation 1 to obtain the sensitivities for our FLUXTAB and the flat fields for our FLATFILE using observations of a flux standard star. We can accomplish this by re-arranging the formula so that it instead reads as,

$$S(\lambda) \times L(X) \times P(X) = \frac{C(\lambda, X)}{J_{model}(\lambda)} \quad (2)$$

Here, we have replaced the source flux density, $F(\lambda)$, with a model spectral energy distribution, $J_{model}(\lambda)$. We can solve for $S(\lambda)$ and the flat fields simultaneously by fitting the functions using the Levenberg-Marquardt least squares minimization algorithm. Solving for the fit simultaneously is possible with data taken at multiple cenwaves and/or FP-POS positions, breaking the degeneracy between the wavelength and the detector position. This method was first described and implemented by Massa et al. (2014) and further refined by Debes et al. (2016). It is implemented in an IDL code¹, which we will refer to as the ‘‘COS FUV Flats and Flux code’’ henceforth.

This code requires one-dimensional extracted spectra (`x1d` files) that have had the shadows from the grid wires in front of the detector (Ely et al., 2011) removed and that have been corrected for the ‘‘impostor’’ features due to geometric distortion at the edges of FUVB. The `x1d` data products were made by processing the raw time-tag event list files, or `rawtags`, through version 3.4.3 of the CalCOS pipeline and utilized a basic FLATFILE containing the grid wire shadows and impostor features, as well as the LP6-era BPIXTAB (Miller et al., in prep), which identifies low and very low response regions that are not included as valid pixels in the COS FUV Flats and Flux code.

Following the process outlined in Equation 2, the net counts in the `x1d` files at each FP-POS position were divided by a spectrophotometric model of our target, WD0308-565 (Bohlin et al., 2014, `wd0308_565_mod_006.dat`), where absorption and emission lines, such as $\text{Ly}\alpha$, were masked out to retain only the continuum. $L(X)$ and $S(\lambda)$ were defined at 20 and 15 regularly spaced points, as was done for previous LPs (see Debes et al. 2016). The fit was then performed using a cubic spline to interpolate between the points for the L-FLAT, while the sensitivity function used a piecewise quadratic interpolation. Each segment was treated independently. This resulted in a one-dimensional L-FLAT for the G160M grating and an average

¹`derive.cos.flats.pro`, written by G. Becker

sensitivity curve. The P-FLAT was considered as noise during the initial fitting procedure and was obtained by dividing out $L(X)$ and $S(\lambda)$ and fitting a spline to the residual. This procedure was then repeated to produce a sensitivity curve for each of the individual cenwaves by holding the raw flat ($L(X) \times P(X)$), one of the products returned by the first run of the COS FUV Flats and Flux code (which includes the `lflat`, `pflat`, `rawflat`, `rawflaterr`, and `sens`), fixed.

Finally, we used a Python script² to project the one-dimensional L-FLAT products from the COS FUV Flats and Flux code at each segment into the second dimension to create a 16384 x 1024 flat-field FITS image (the FLATFILE). We then scaled the individual sensitivity curves to a reference time in the TDSTAB (`52m2056hl_tds.fits`) with a separate code³ to reflect the COS FUV detector's sensitivity at launch. These “backed-out” cenwave and segment-dependent curves were assembled into a FITS table (the FLUXTAB).

Our procedure was iterative due to the interdependence between the DISPTAB (Fischer et al. 2023), LAMPTAB (Indriolo et al. 2023), the spectral extraction reference files—the XTRACTAB for the BOXCAR extraction algorithm, and the TWOZXTAB, PROFTAB, and TRACETAB for TWOZONE extraction algorithm (Frazer et al., in prep)—and the FLATFILE. We produced an initial FLATFILE from data processed with BOXCAR extraction, using the LP4 LAMPTAB and DISPTAB files and a first iteration of the LP6 XTRACTAB file. An LP6 LAMPTAB and DISPTAB, as well as an updated XTRACTAB, were then made using data that had been processed with the first version of the LP6 FLATFILE. A second iteration of the LP6 FLATFILE and the LP6 FLUXTAB was created with the new LAMPTAB, DISPTAB, and XTRACTAB. We repeat these steps with TWOZONE extraction to obtain the LP6 TRACETAB, PROFTAB, and TWOZXTAB reference files. In summary, two iterations using BOXCAR extraction were done, followed by two with TWOZONE extraction until the results converged with residuals less than 0.4% everywhere in the L-flat arrays.

As a technical verification of our newly derived FLATFILE for G160M, we compared the one-dimensional L-FLATS versus XCORR for each segment at LP6 and at LP4, where G160M was previously placed on the detector, as shown in Figures 1 and 2. The LP6 L-FLAT generally follows the shape of the LP4 L-FLAT, with some variations in amplitude. Except at the edges, the LP6 and LP4 flat agree mostly to within 2% of each other, which is in line with what we see between other lifetime positions. Similarly, to validate the FLUXTAB, we plotted the TDS-corrected sensitivity curves against the wavelength at LP6 and at LP4 for each central wavelength and segment. An example of these plots is shown for cenwave 1533, FUVB in Figure 3, while the plots for the remainder of the cenwaves and segments can be found in the appendix (Figures A1 through A11). The results of this test demonstrate that the sensitivity at LP6 for FUVB is approximately 5-10 % higher than

²`updateLP6flat.script.py`, written by R.Sankrit and L.Miller

³`updateLP6phot.script.py`, written by R.Sankrit and L.Miller

at LP4. For FUVB, there is greater sensitivity at bluer wavelengths than at LP4, and at redder wavelengths, the sensitivity is less than at LP4.

As an additional test, we compared observations of WD0308-565 at LP4 (PID 15458, 1533 and PID 14910, 1577-1623) and LP6 (PID 16906, 1533-1623) against their respective CALSPEC models, as sampled in Figures 4, 5, 6, and 7 for cenwaves 1533 and 1577 (see the appendix for cenwaves 1589-1623, shown in Figures A12 through A19). These inspections provide us with a consistency check to validate that the appropriate CALSPEC model was used to amend a selected FLUXTAB. The average residuals for both LP6 and LP4 fall mostly below 1%, as expected. However, we note that the residuals are greater for LP4 at cenwave 1533, FUVB since the CALSPEC model used to derive the LP4 FLUXTAB at this mode (G160M/FUVB) was GD71, not WD0308-565.

4. Scientific Validation of the Flux Calibration

We performed three assessments to confirm that our newly derived FLATFILE and FLUXTAB yielded scientifically accurate flux-calibrated spectra. These tests were done with data re-calibrated through the CalCOS pipeline using the TWOZONE extraction algorithm and all the LP6 reference files. A list of these datasets is available in Table 2.

In our first test, as shown in Figures 8 and 9, we confirmed that the flat field is correctly applied so that each cenwave provides the same number of counts at each wavelength, demonstrating the spectra have been corrected for elements of the detector response that vary slowly with the position.

For the second test, we contrasted data taken of GD71 at LP4 and LP6 against the source flux model for this COS standard star. We require our absolute flux calibration to be within 5% of the accepted spectrophotometric model flux value. The results are shown in Figures 10 through 14. In general, across all of the cenwaves, the difference between the model and the flux for LP6 falls within this constraint, with the average residual being 0.59%. This is close to the same average residual we find for LP4, at 0.31%. FUVB, cenwave 1600 at GD71 was removed from our scientific testing since the observation had problems, with the target not being entirely centered after the guide stars were re-acquired (see Section 2), which led to a loss of counts.

Finally, in our third test, we use data taken of AV 75, an O5.5 blue super giant in the Small Magellanic Cloud (SMC), at LP4 and LP6 to verify that the spectra agree to within 2% of each other, which is our requirement for relative flux calibration. Although AV75 is not a standard flux calibration star, it has often been observed as part of wavelength calibration programs for COS, shows little variability in the continuum, and is one of the few stars with observations available at all lifetime positions. The resulting plots are shown in Figures 15 and 16. A majority of the residual points fall within our 2% boundary for both FUVB and FUVB in the wavelength range, except where there are deep absorption features and at lines where variability is expected to occur due to stellar winds (which can be seen at 1550 Å for FUVB).

Table 2. FUV Scientific Testing Datasets

Lifetime Position	Target	Central Wavelength(s)	Segment(s)	PID	PI
LP4	GD71	1577-1623	FUVA	14910	M.Rafelski
LP4	GD71	1533	FUVA	15458	E.Frazer
LP6	GD71	1533-1623	FUVA	16906	E.Frazer
LP4	AV75	1623	FUVA/FUVB	15366	A.Fox
LP6	AV75	1623	FUVA/FUVB	16907	N.Kerman

Table 3. Files Delivered to CRDS

Filename	Observation Mode	Activation Date	UseAfter Date
69d2108sl_phot.fits	FUV/G160M/LP6	2022-09-14	2017-10-02
69d21090l_flat.fits	FUV/G160M/LP6	2022-09-14	1996-10-01

5. Reference Files Delivered and Conclusion

We created a new FLUXTAB and FLATFILE for COS FUVA and FUVB at G160M, central wavelengths 1533-1623, for use at LP6. We scientifically tested the flux calibration of the new LP6 reference files by re-processing data of GD71 and verifying that the residuals, compared to the CALSPEC models, were within our 5% absolute flux requirement. In addition, we validated that the FLUXTAB and FLATFILE produce spectra of the same standard star with flux differences of less than or equal to 2% with data of AV75 from LP4 and LP6. The FLUXTAB and FLATFILE were delivered to the HST Calibration Reference Data System (CRDS) on September 13th, 2022, for use in standard CalCOS reduction. The filenames and associated use-after and activation dates are listed in Table 3. The FLUXTAB has since been superseded due to updates in the TDSTAB breakpoints (Hernandez et al., in prep). Figures 17 and 18 demonstrate an example of the differences in the sensitivity curves between what was derived in this ISR (69d2108sl_phot.fits) and the most recent version of the FLUXTAB (83j204511_phot.fits). We have verified that the changes in the newest FLUXTAB result in precise and accurate flux calibration.

Change History for COS ISR 2023-16

Version 1: 25 September 2024- Original Document

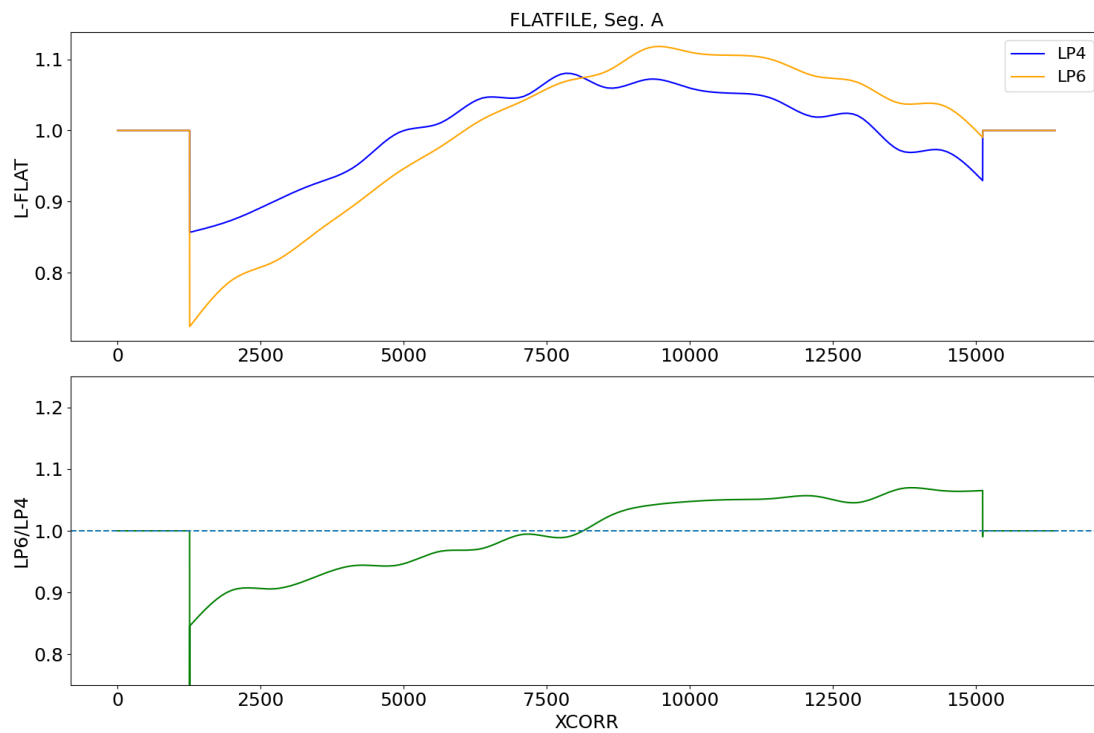


Figure 1.: The top panel shows the one-dimensional G160M FUV L-Flat curves for LP6 (yellow) and LP4 (blue). The gridwire shadows and imposter features have been divided out. The bottom plots the ratio between the LP6 L-FLAT and the LP4 L-FLAT.

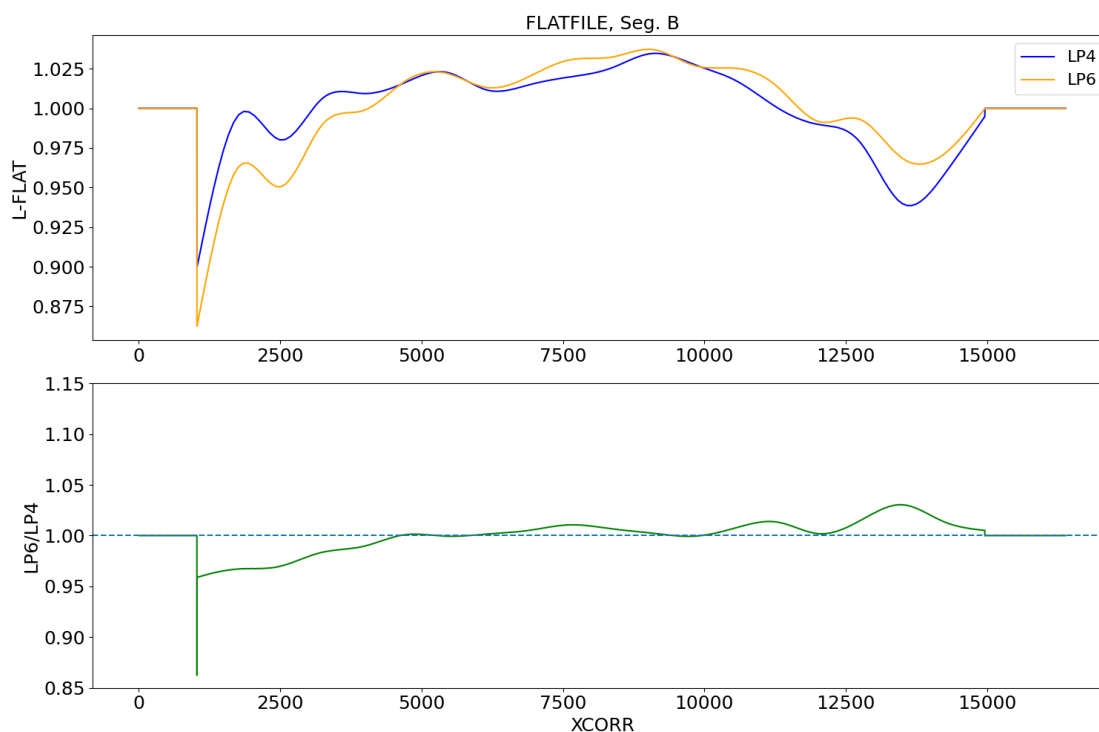


Figure 2.: The same as Fig.1, but for G160M/FUVB

References

- Ely, J., Massa, D., Ake, T., et al. 2011, COS Instrument Science Report 2011-03, “COS FUV Gridwire Flat Field Template”
- Sahnow, D., Oliviera, C., Aloissi, A., et al. 2011, COS Instrument Science Report 2011-5, “Gain Sag in the FUV detector of the Cosmic Origins Spectrograph”
- Massa, D., Ely, J., Osten, R., et al. 2013, COS Instrument Science Report 2013-09, “Updated Absolute Flux Calibration of the COS FUV Modes”
- Bohlin, R., Gordon, K. D., Tremblay, P.-E. 2014, PASP, 126, 711
- Debes, J. H., Becker, G., Roman-Doval, J., et al. 2016, COS Instrument Science Report 2016-15, “Third COS FUV Lifetime Calibration Program: Flatfield and Flux Calibrations”
- Fischer, W.J., Dieterich, S., Frazer, E.M., et al. 2022, COS Instrument Science Report 2022-03, “Summary of COS Calibration for the Lifetime Position 5 Era”
- Indriolo, N., Fischer, W., Frazer, E., et al. 2023, COS Instrument Science Report 2023-09, “Creation of the LAMPTAB reference file for use at Lifetime Position 6”
- James, B., Rafelski, M., Oliviera, C., et al. 2023, COS Instrument Science Report 2023-10, “LP5 Exploratory Study”
- James, B., Rafelski, M., Dashtamirova, D., et al. 2023, COS Instrument Science Report 2023-15, “LP6 Exploratory Study”

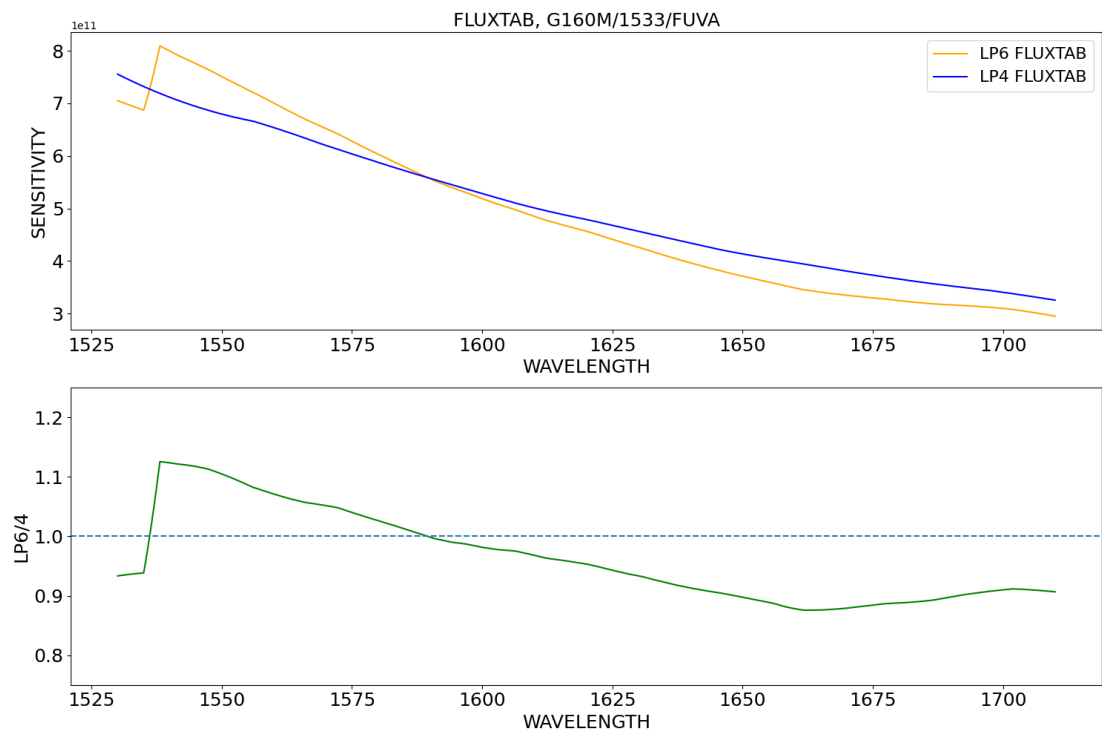


Figure 3.: The top panel shows the sensitivity curve for G160M/1533 FUVA at LP6 (yellow) and LP4 (blue). The bottom plots the ratio between these two sensitivity curves.

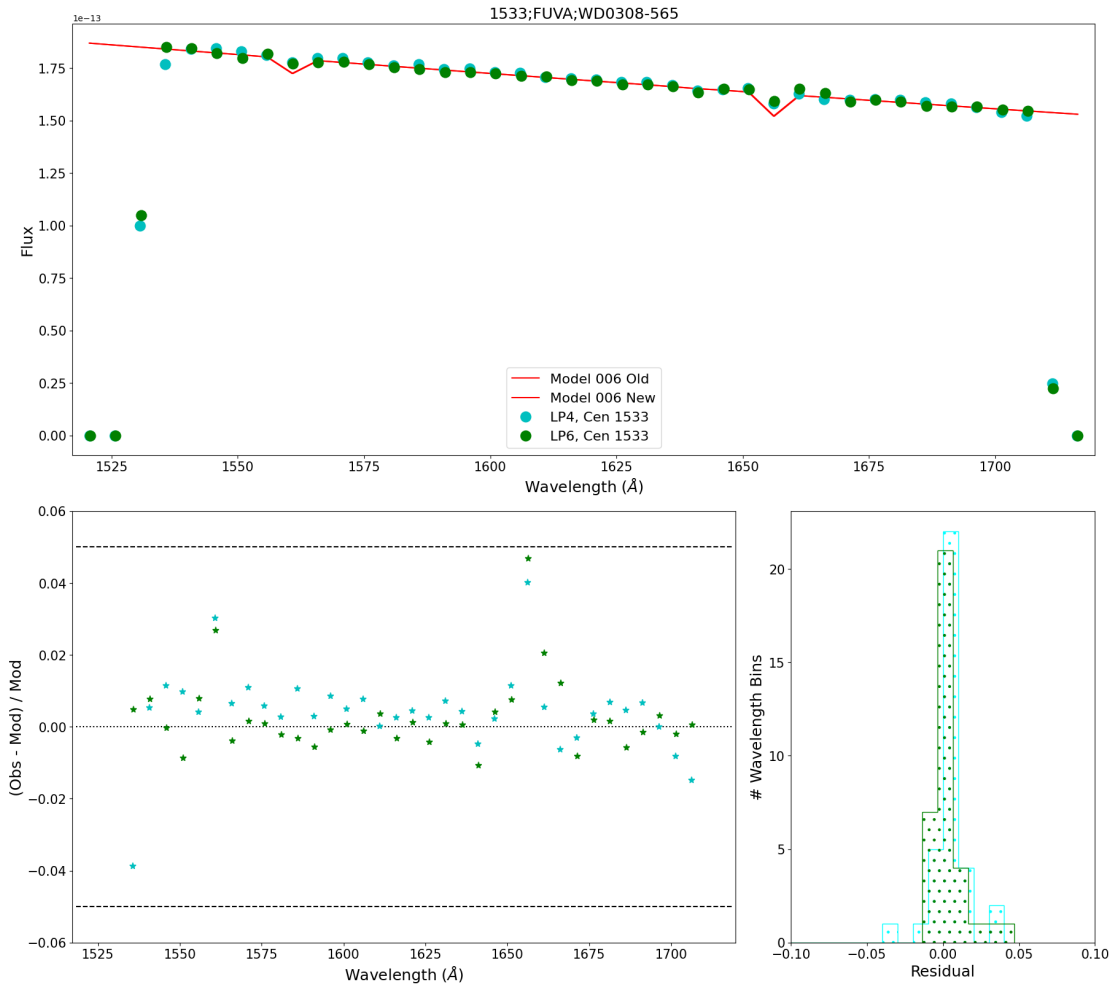


Figure 4: The top panel shows observed spectra of WD0308-565 obtained at LP6 in program 16906 (filled green circles) and at LP4 in program 15458 (filled cyan circles) for central wavelength 1533, FUV overlaid on CALSPEC models that have been interpolated to the data (red and orange lines). The spectrum and models are binned by 5 angstroms. The bottom left panel shows the residual differences between the observation and models. The dashed line is our required accuracy for absolute flux calibration of 5%. The bottom right panel shows the histograms of the residuals. Note that the residuals for LP4 are higher than that for LP6 since the FLUXTAB at LP4 was derived using GD71 and not WD0308-565.

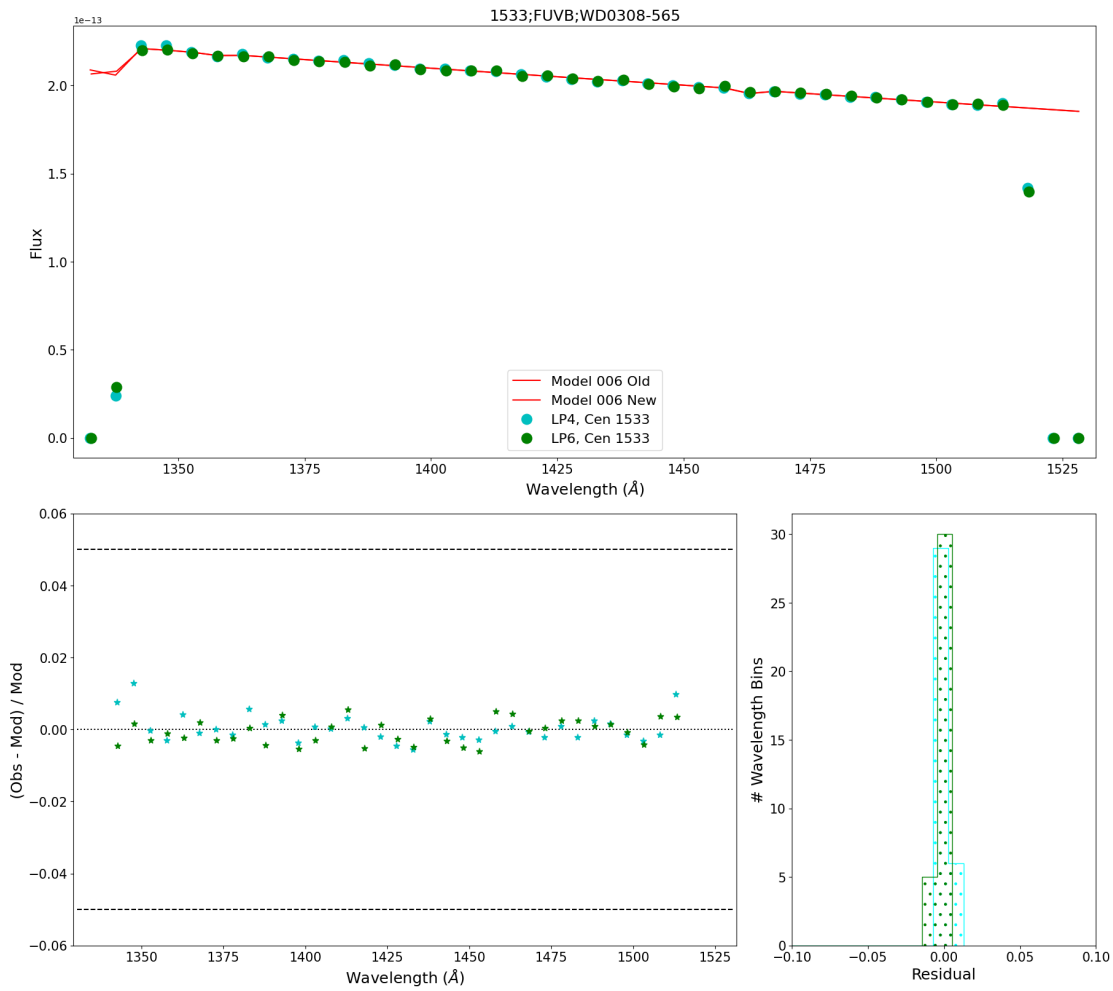


Figure 5.: The same as Fig. 4, but for G160M/1533/FUVB.

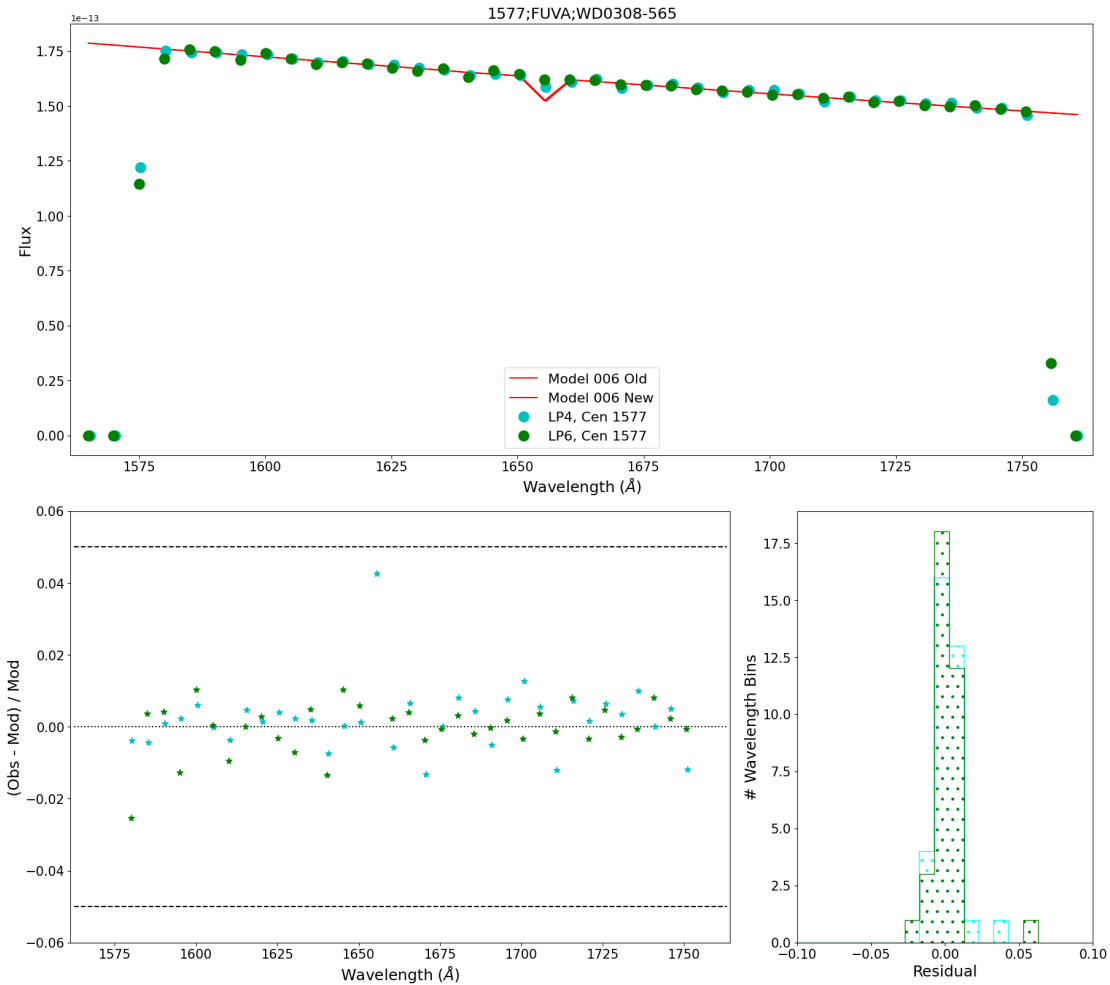


Figure 6: The top panel shows observed spectra of WD0308-565 obtained at LP6 in program 16906 (filled green circles) and at LP4 in program 14910 (filled cyan circles) for central wavelength 1577, FUV overlaid on CALSPEC models that have been interpolated to the data (red and orange lines). The spectrum and models are binned by 5 angstroms. The bottom left panel shows the residual differences between the observation and models. The dashed line is our required accuracy for absolute flux calibration of 5%. The bottom right panel shows the histograms of the residuals. Note that the residuals for LP4 are higher than that for LP6 since the FLUXTAB at LP4 was derived using GD71 and not WD0308-565.

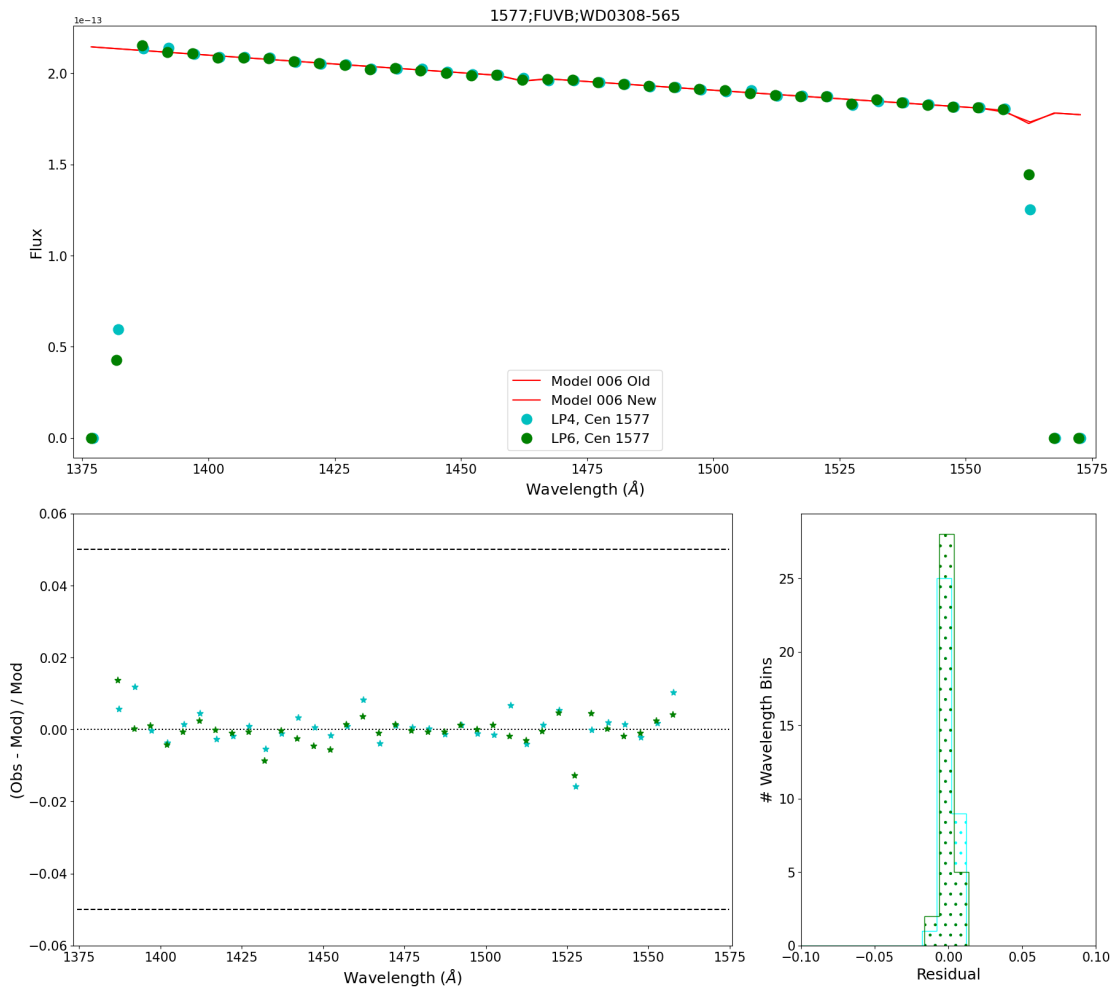


Figure 7.: The same as Fig. 6, but for G160M/1577/FUVB.

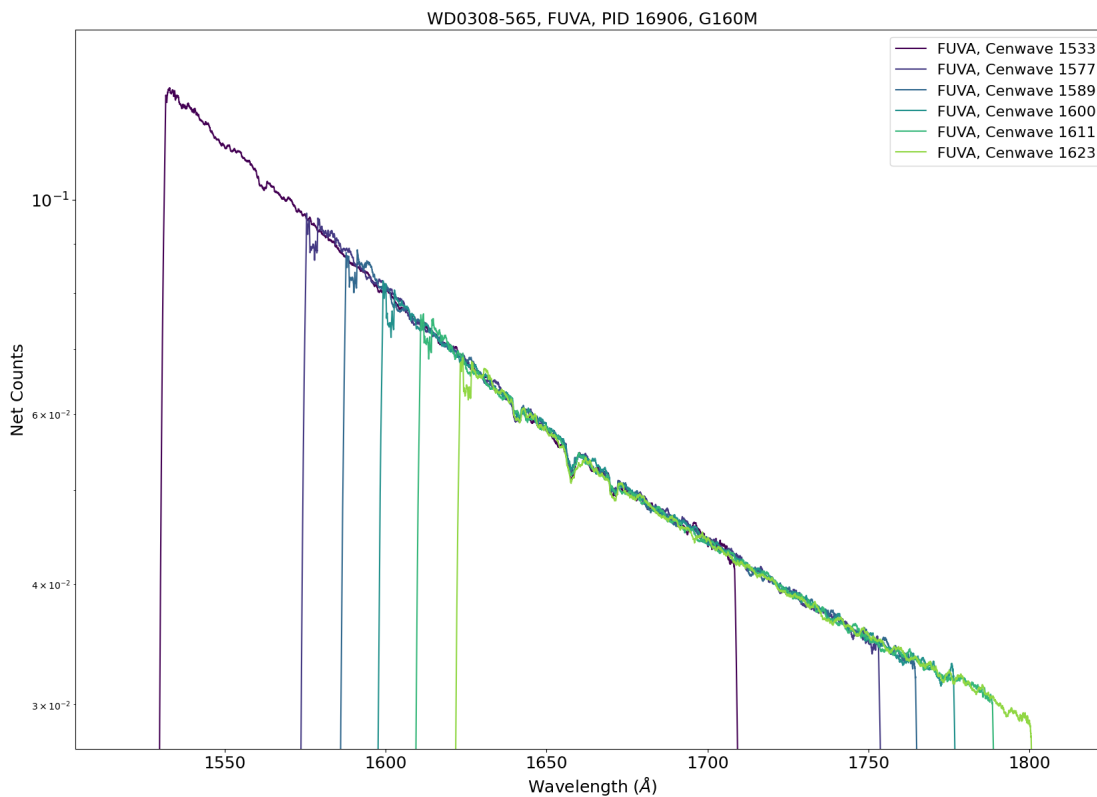


Figure 8.: The net counts versus the wavelength for WD0308–565 FUVA across all of the G160M cenwaves, using data from PID 16906 that has been re-calibrated using the LP6 reference files. Each cenwave provides the same number of counts at each wavelength, demonstrating the effectiveness of the newly derived flat correction.

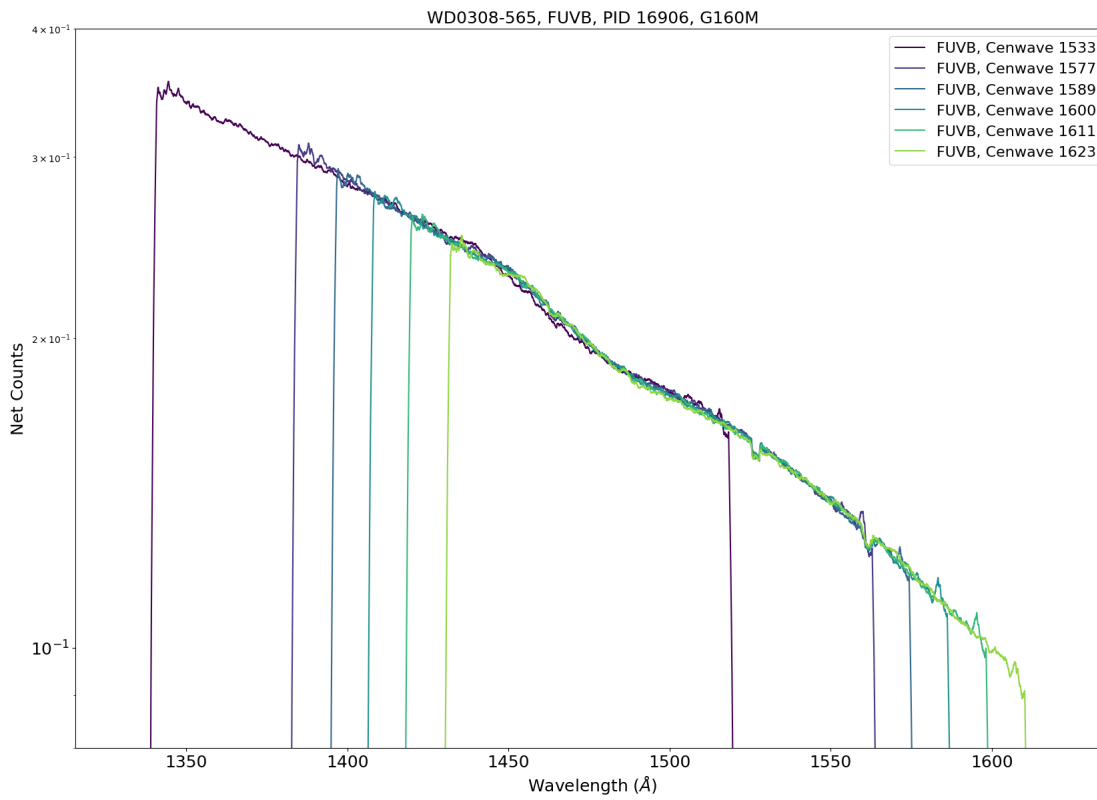


Figure 9.: The same as Fig. 8, but for G160M/FUVB.

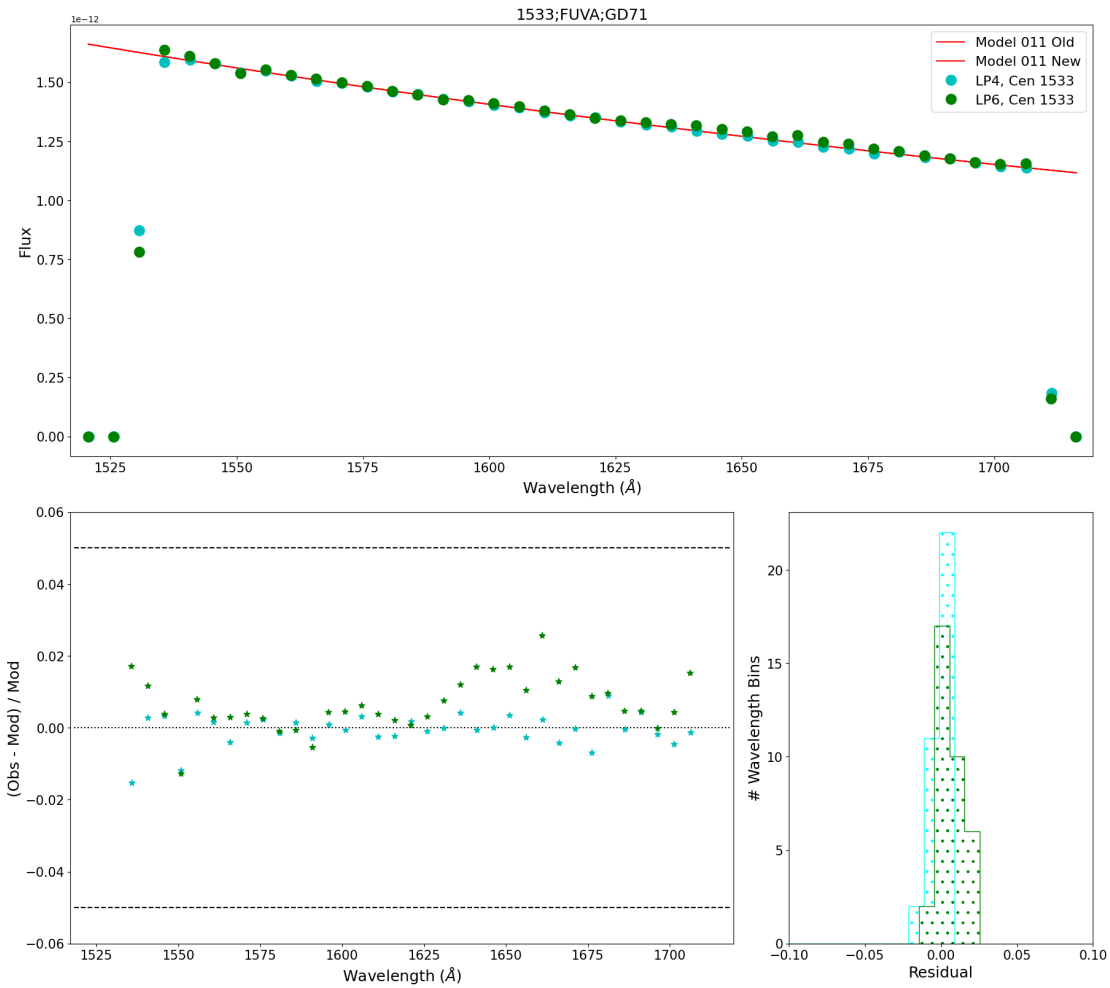


Figure 10.: The top panel shows observed spectra of GD71 obtained at LP6 in program 16906 (filled green circles) and at LP4 in program 15458 (filled cyan circles) for central wavelength 1533, FUVa overlaid on CALSPEC models that have been interpolated to the data (red and orange lines). The spectrum and models are binned by 5 angstroms. The bottom left panel shows the residual differences between the observation and models. The dashed line is our required accuracy for absolute flux calibration of 5%. The bottom right panel shows the histograms of the residuals.

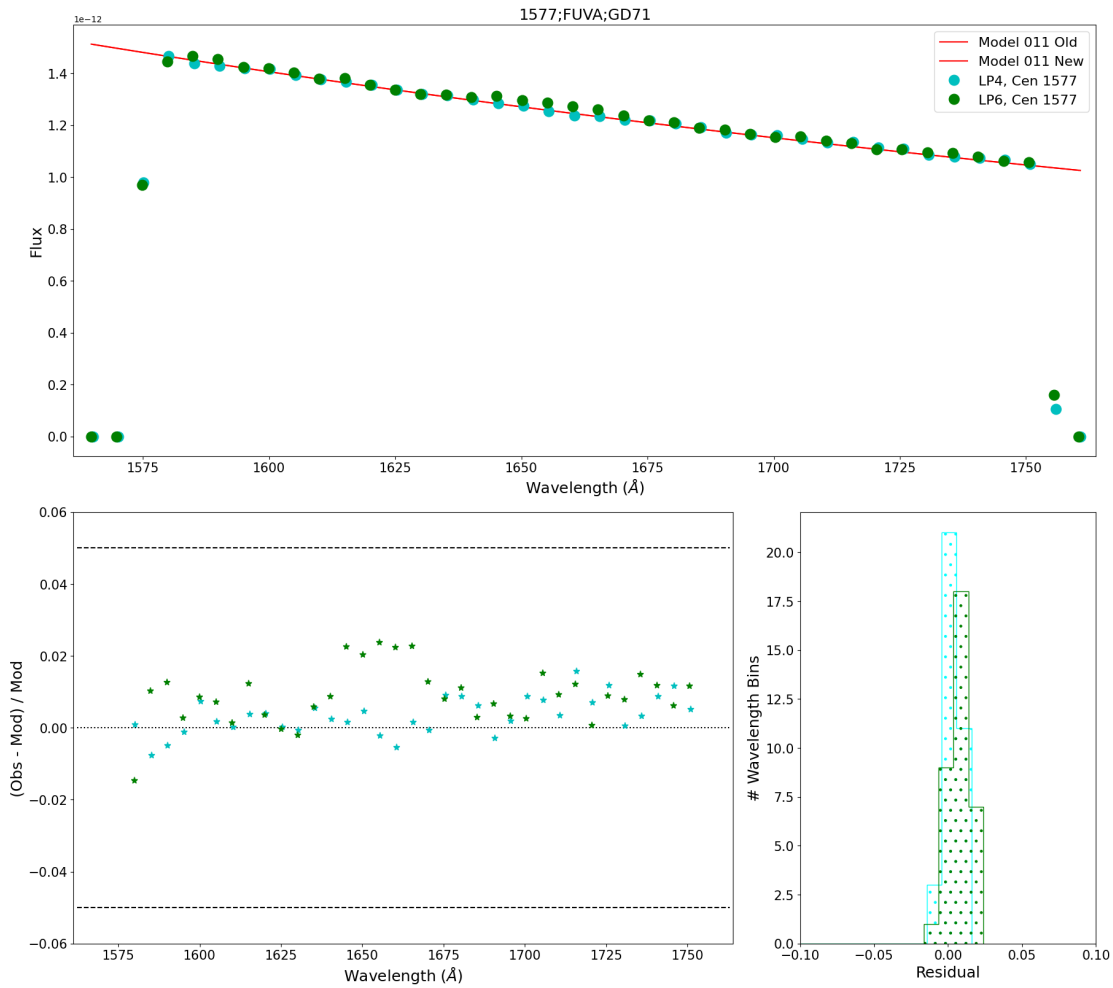


Figure 11.: The top panel shows observed spectra of GD71 obtained at LP6 in program 16906 (filled green circles) and at LP4 in program 14910 (filled cyan circles) for central wavelength 1577, FUVA overlaid on CALSPEC models (red and orange lines) that have been interpolated to the data. The spectrum and models are binned by 5 angstroms. The bottom left panel shows the residual differences between the observation and models. The dashed line is our required accuracy for absolute flux calibration of 5%. The bottom right panel shows the histograms of the residuals.

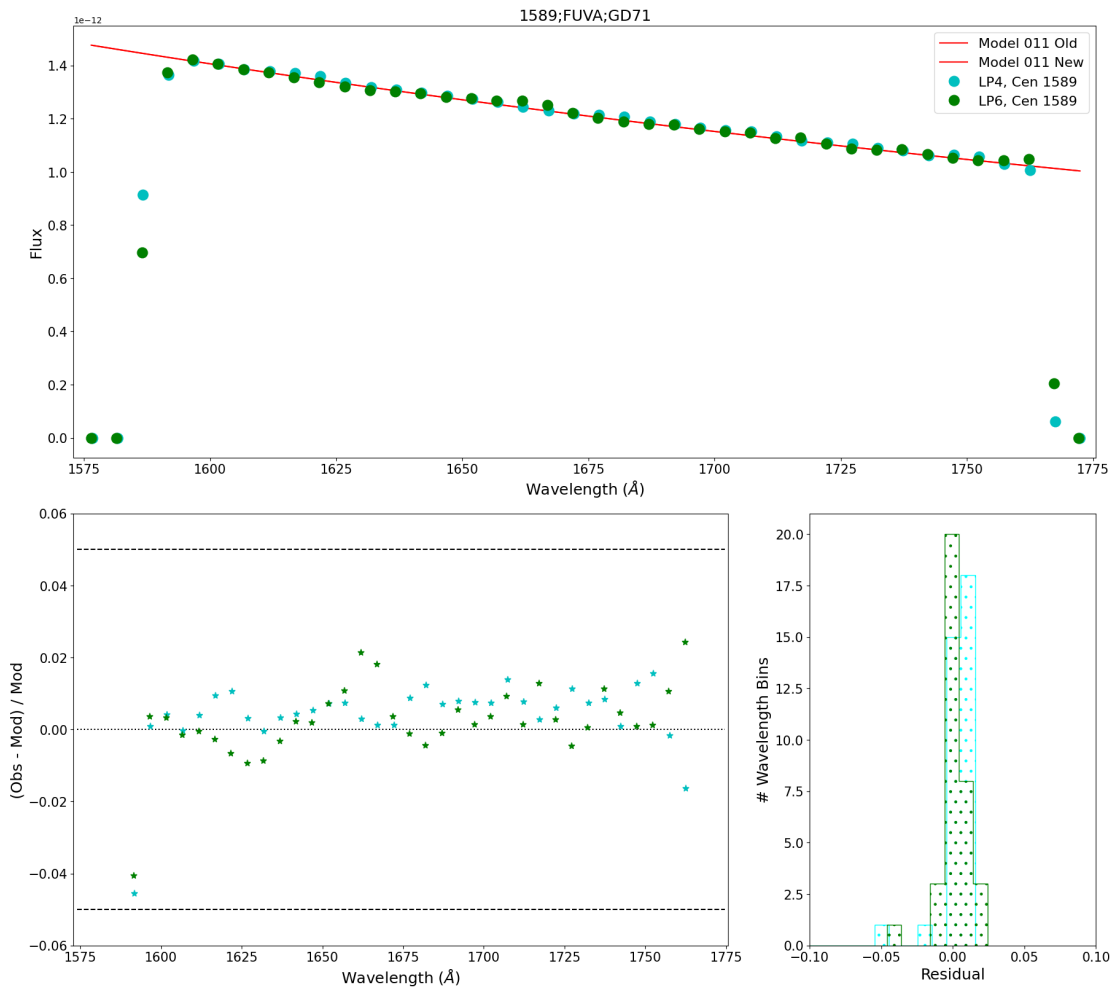


Figure 12.: The same as Fig. 11, but for G160M/1589/FUVA.

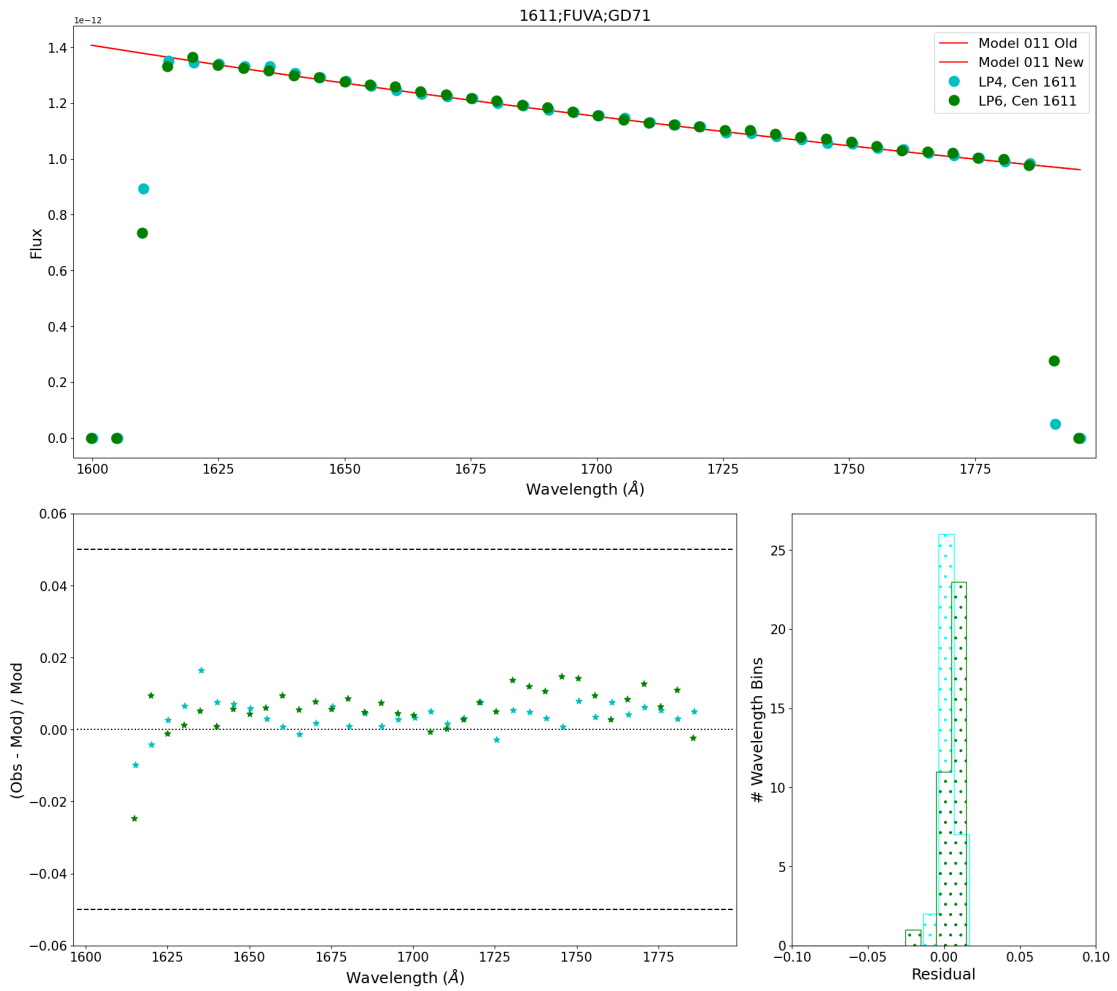


Figure 13.: The same as Fig. 11, but for G160M/1611/FUVA.

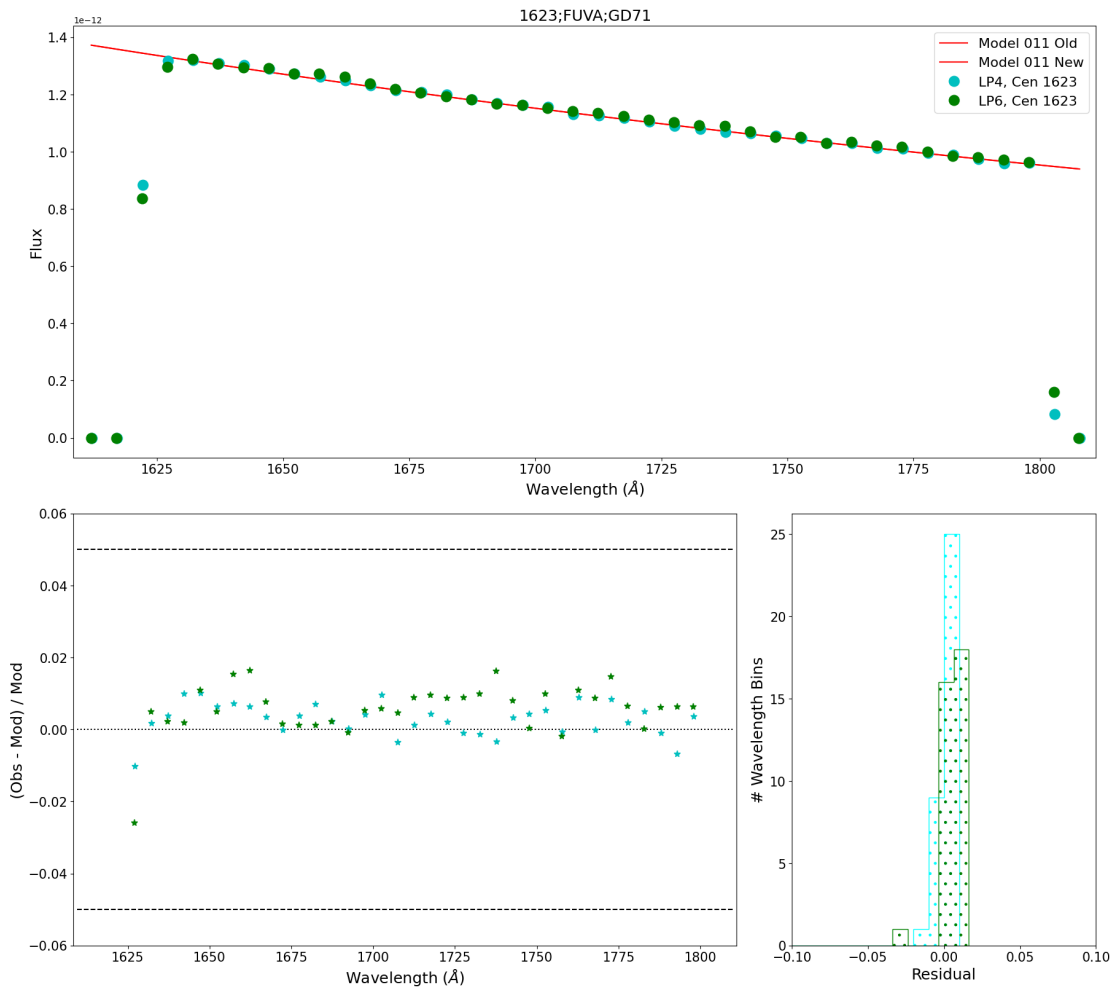


Figure 14.: The same as Fig. 11, but for G160M/1623/FUVA.

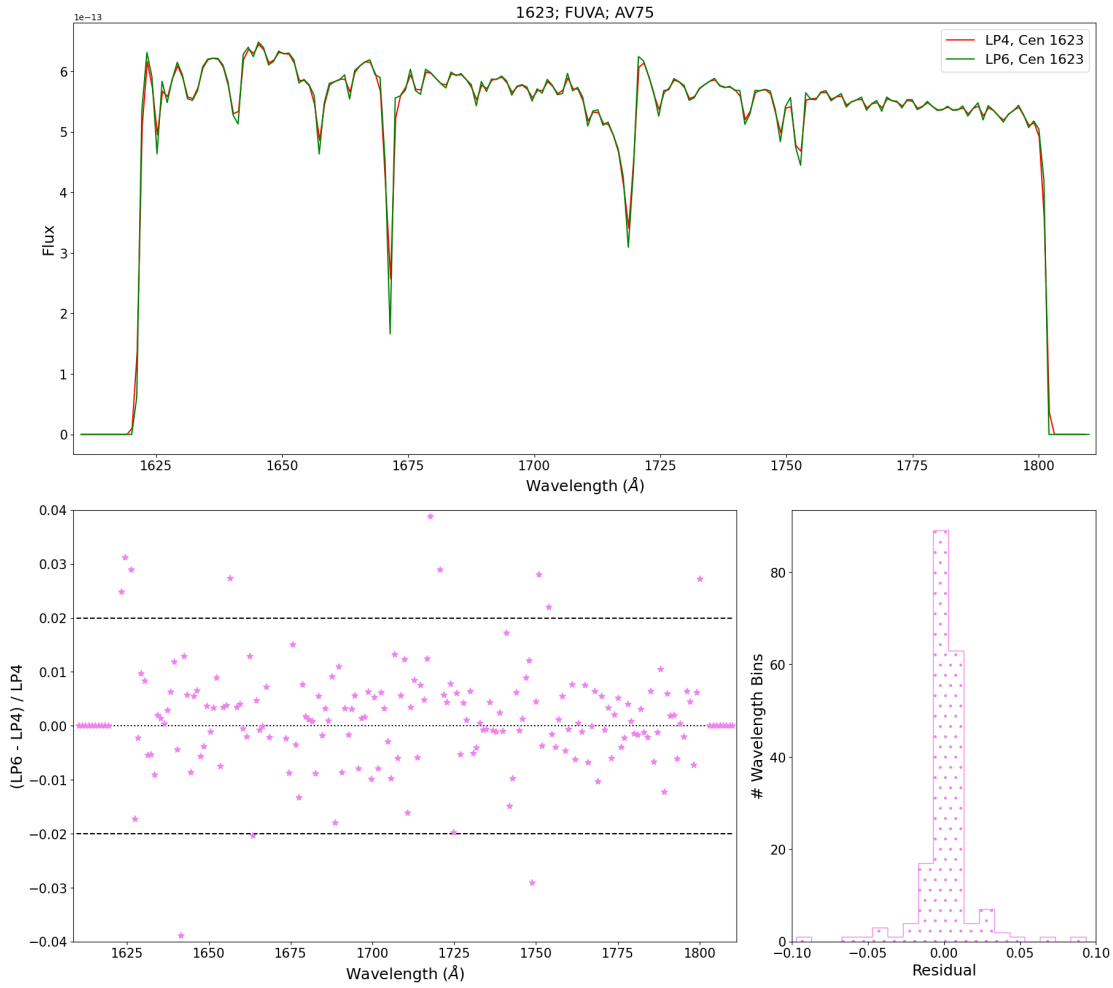


Figure 15.: The top panel shows observed spectra of the blue supergiant AV75 obtained at LP6 in program 16907 (green line) and at LP4 in program 15366 (red line) for central wavelength 1623, FUV A. The spectrum and models are binned by 1 angstrom. The bottom left panel shows the residual differences between the LP6 and LP4 data. The dashed line is our required accuracy for relative flux calibration of 2%. The bottom right panel shows the histograms of the residuals.

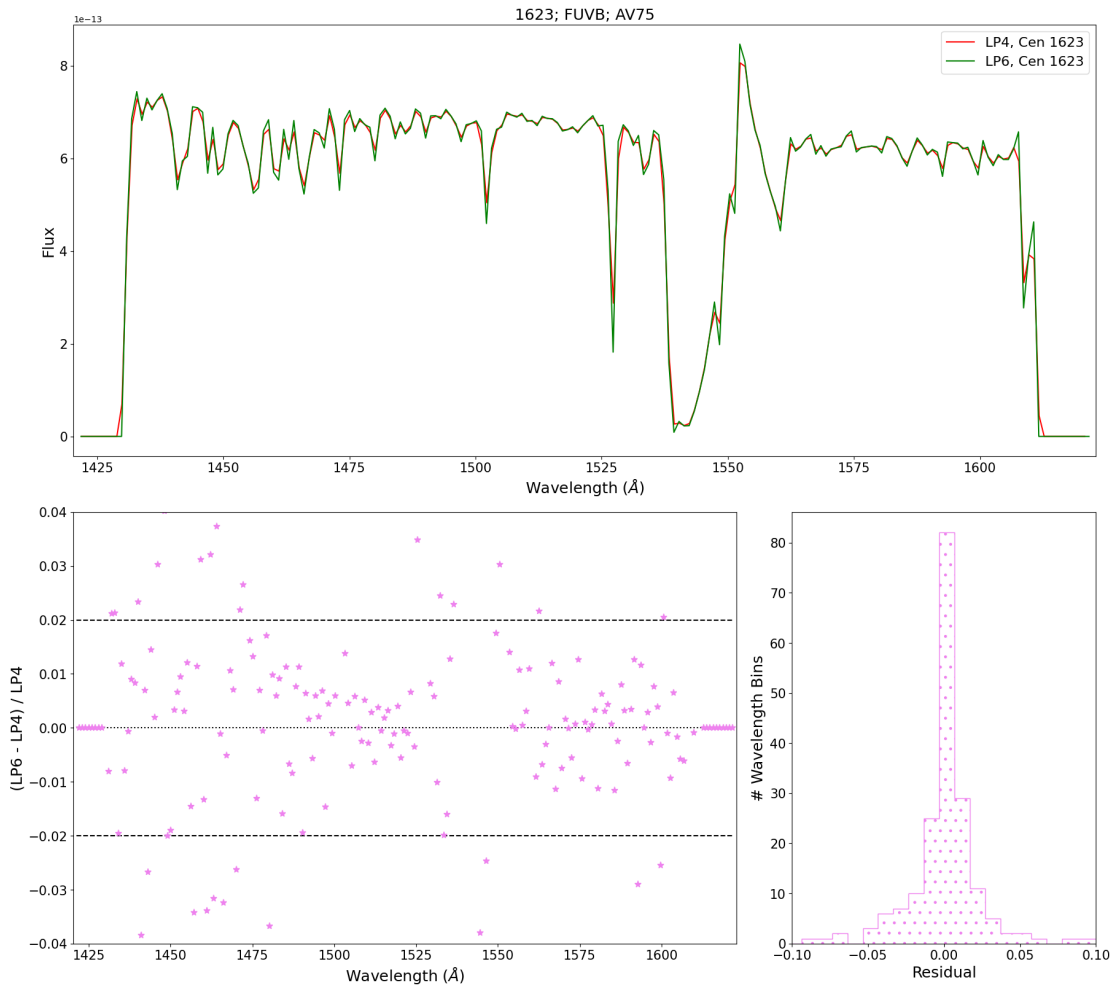


Figure 16.: The same as Fig. 15, but for G160M/1623/FUVB. The discrepancy seen at 1550 angstroms is due to variability resulting from stellar winds.

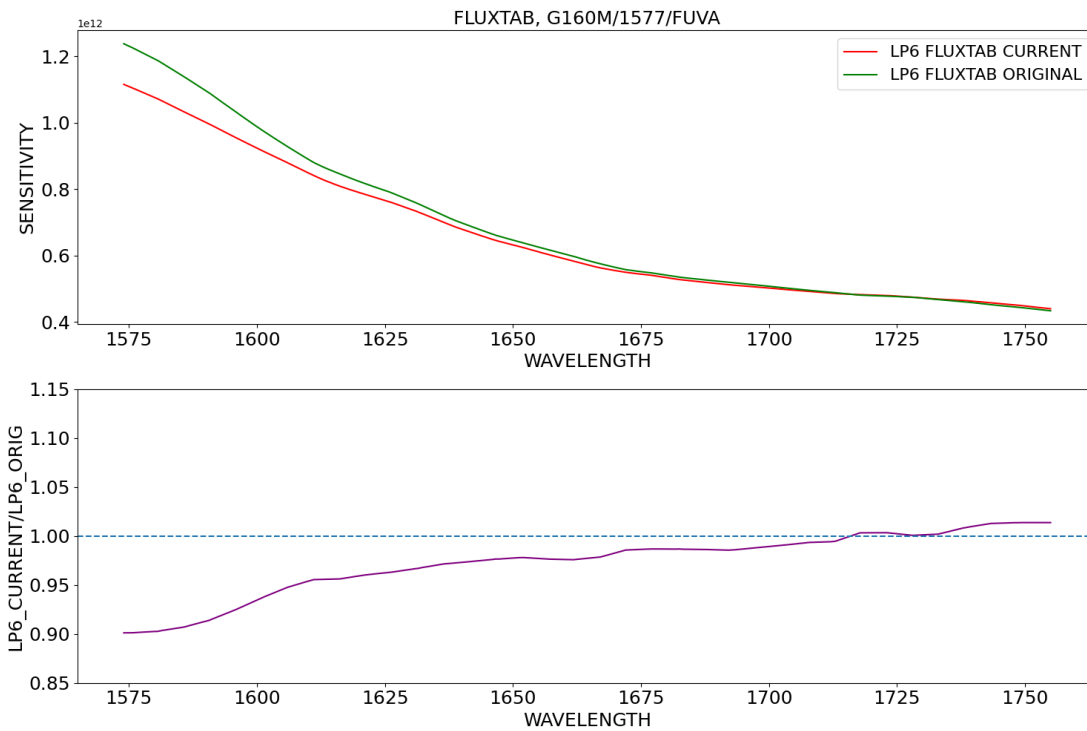


Figure 17.: The top panel shows the sensitivity curve for G160M/1577 FUVA for the original LP6 FLUXTAB (69d2108sl_phot.fits, green) and the most recent LP6 FLUXTAB (83j20451l_phot.fits, red) backed out using the newest TDSTAB. The bottom plots the ratio between these two sensitivity curves.

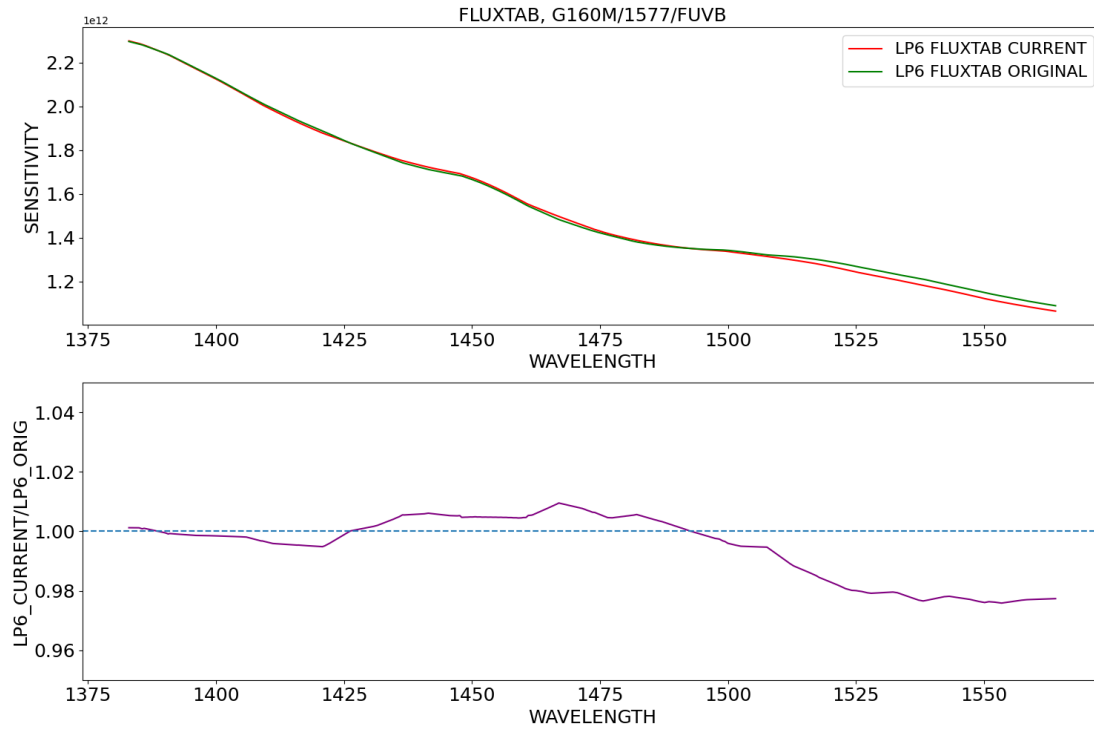


Figure 18.: The same as Fig. 17, but for G160M/1577/FUVB.

Sankrit, R., Fischer, W., Frazer, E., et al. 2023, COS Instrument Science Report 2023-25, “Overview of COS Lifetime Position 6 Calibration”

Fischer, W.J., Frazer, E., Indriolo, N., et al. 2023, COS Instrument Science Report 2023-28, “Derivation of the COS FUV Dispersion Solutions at Lifetime Position 6”

Frazer, E., Miller, L., Sankrit, R. et al., in prep

Hernandez, J. and Frazer, E., in prep

Miller, L., Frazer, E., Hasselquist, S., and Rowlands, K., in prep

Appendix

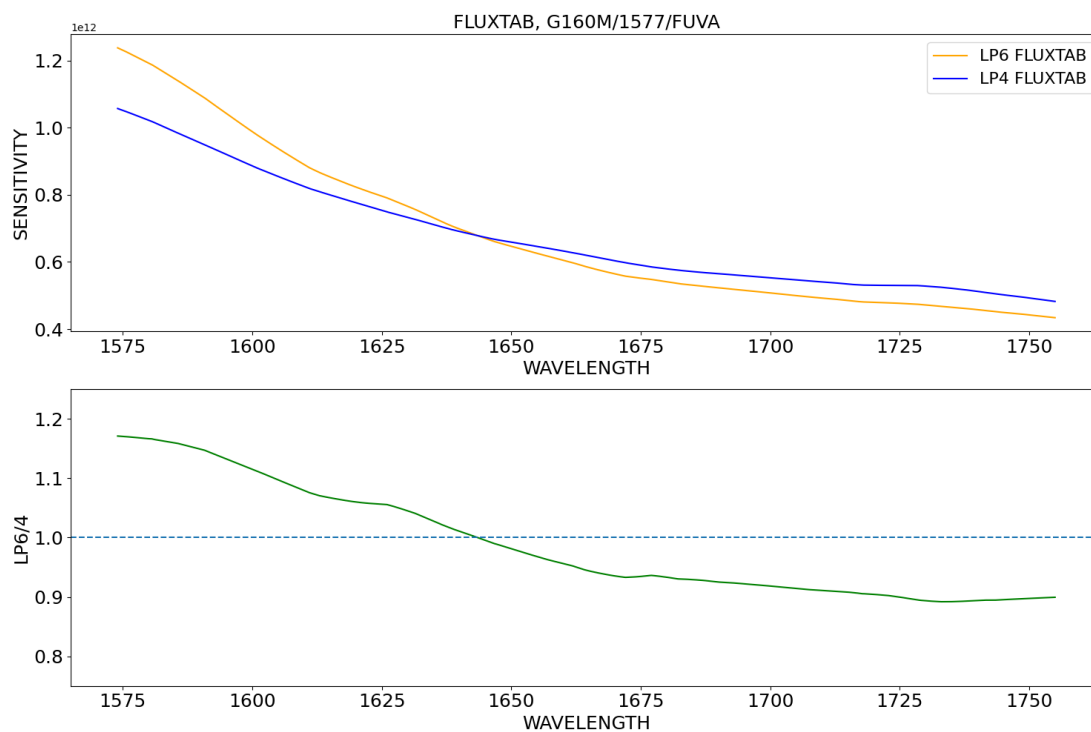


Figure A1.: The same as Fig. 3, but for G160M/1577/FUVA.

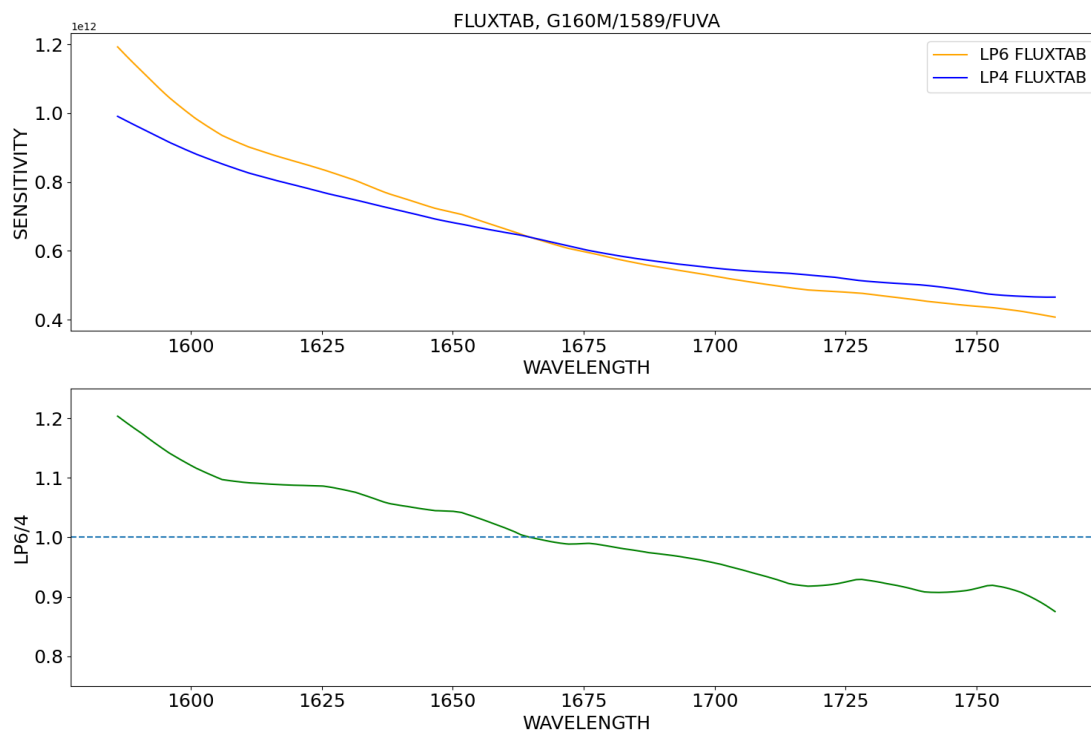


Figure A2.: The same as Fig. 3, but for G160M/1589/FUVA.

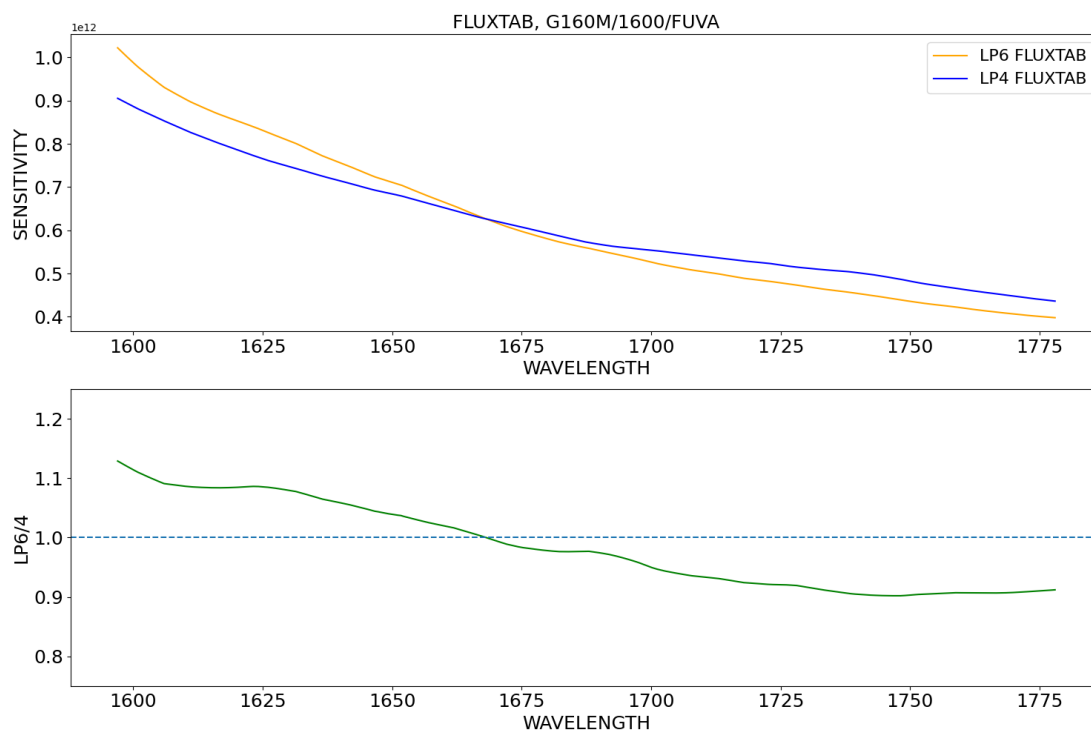


Figure A3.: The same as Fig. 3, but for G160M/1600/FUVA.

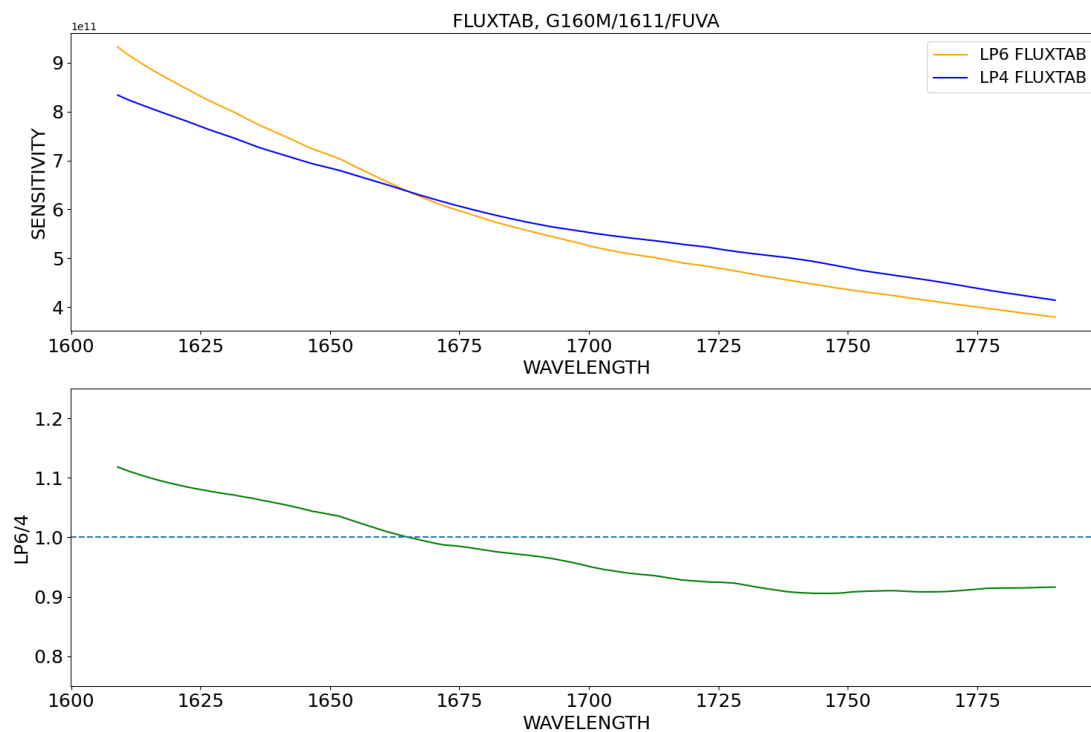


Figure A4.: The same as Fig. 3, but for G160M/1611/FUVA.

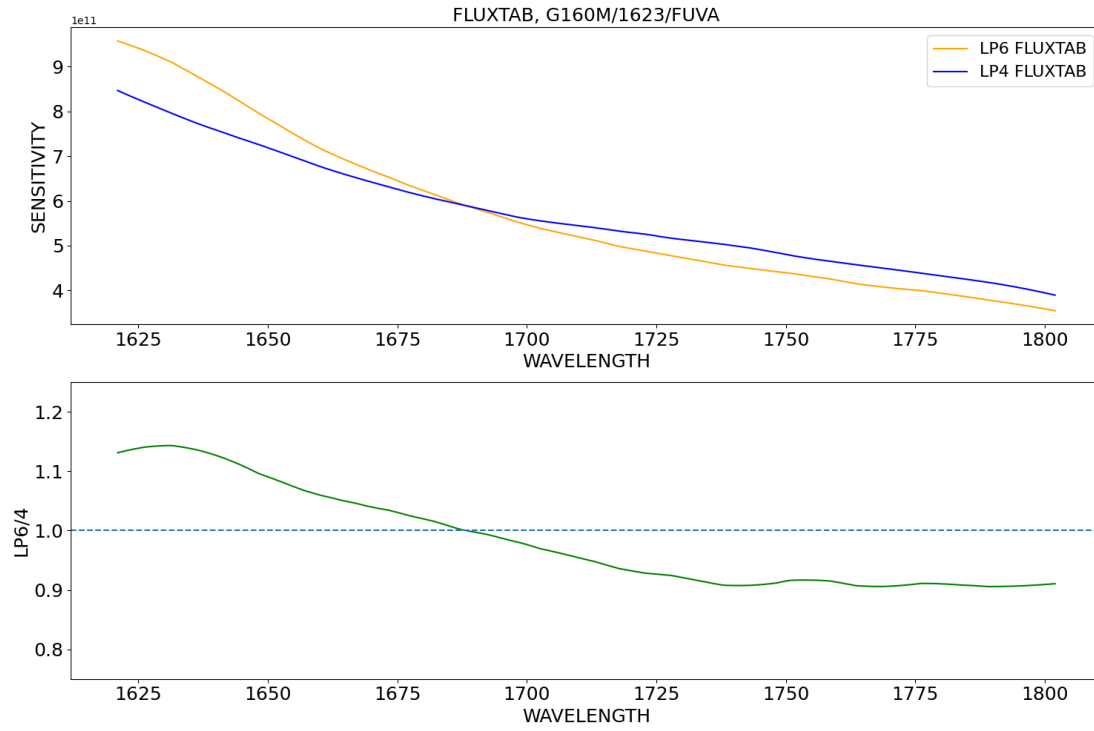


Figure A5.: The same as Fig. 3, but for G160M/1623/FUVA.

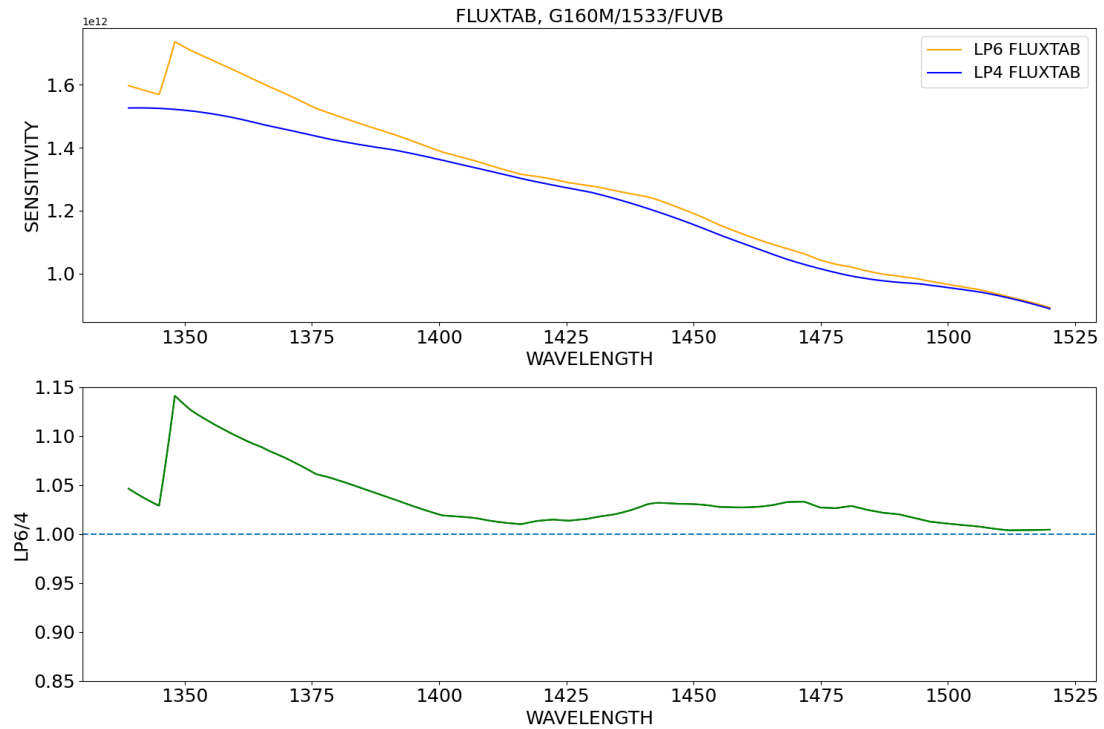


Figure A6.: The same as Fig. 3, but for G160M/1533/FUVB.

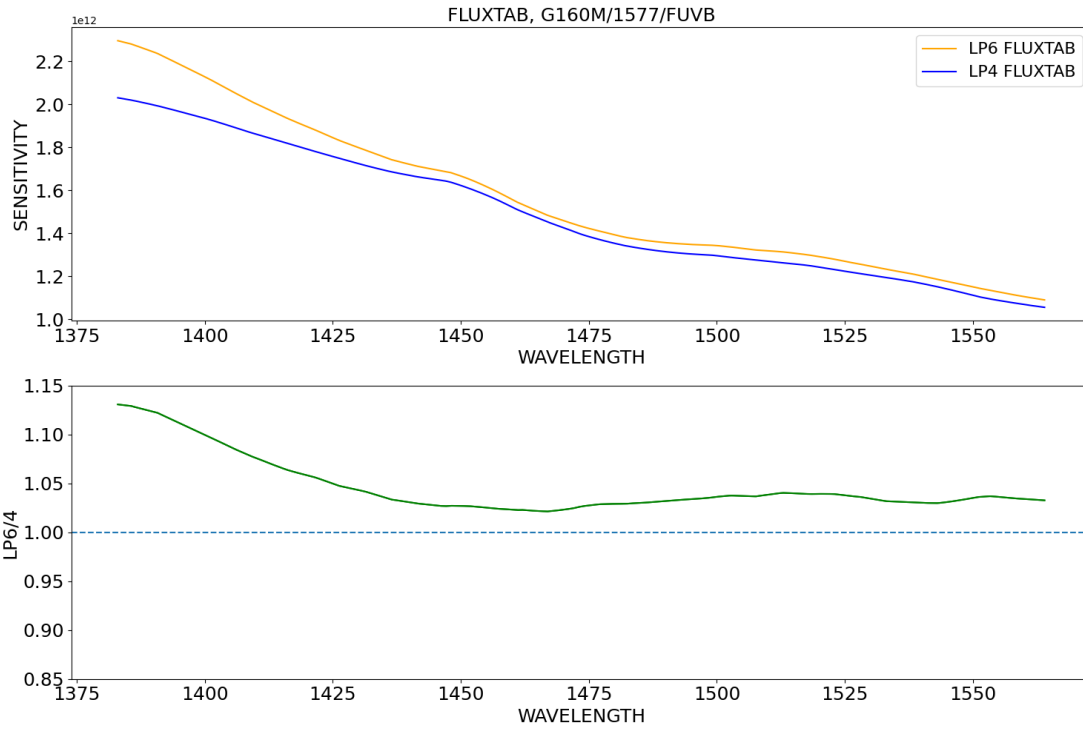


Figure A7.: The same as Fig. 3, but for G160M/1577/FUVB.

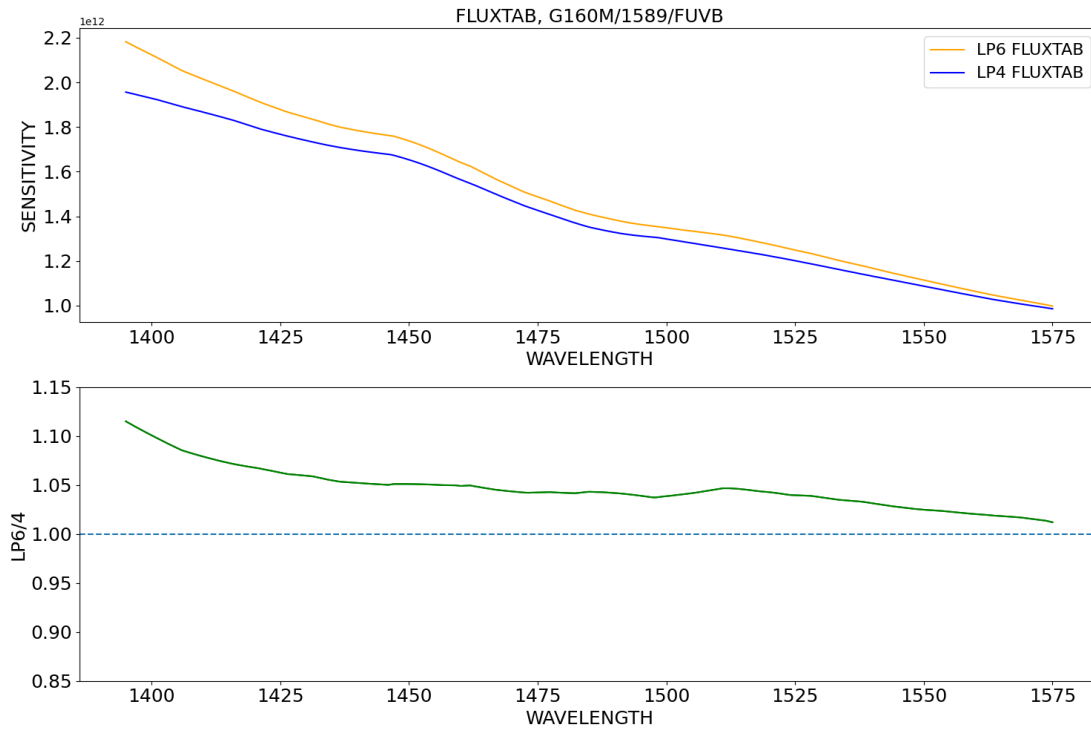


Figure A8.: The same as Fig. 3, but for G160M/1589/FUVB.

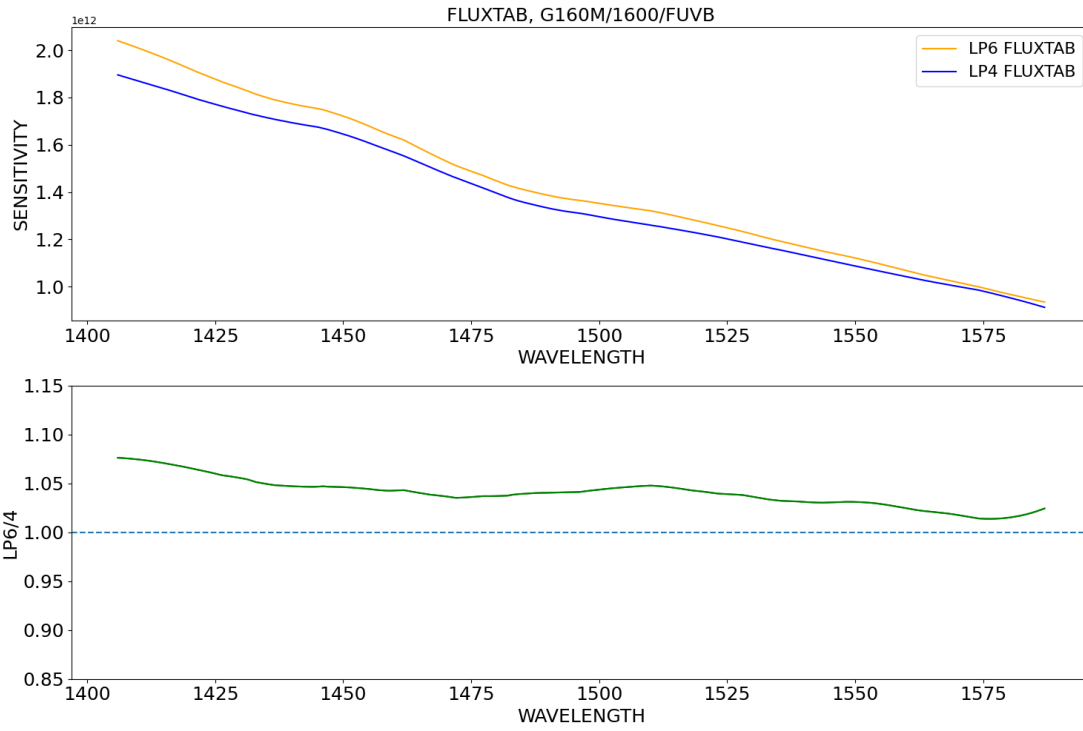


Figure A9.: The same as Fig. 3, but for G160M/1600/FUVB.

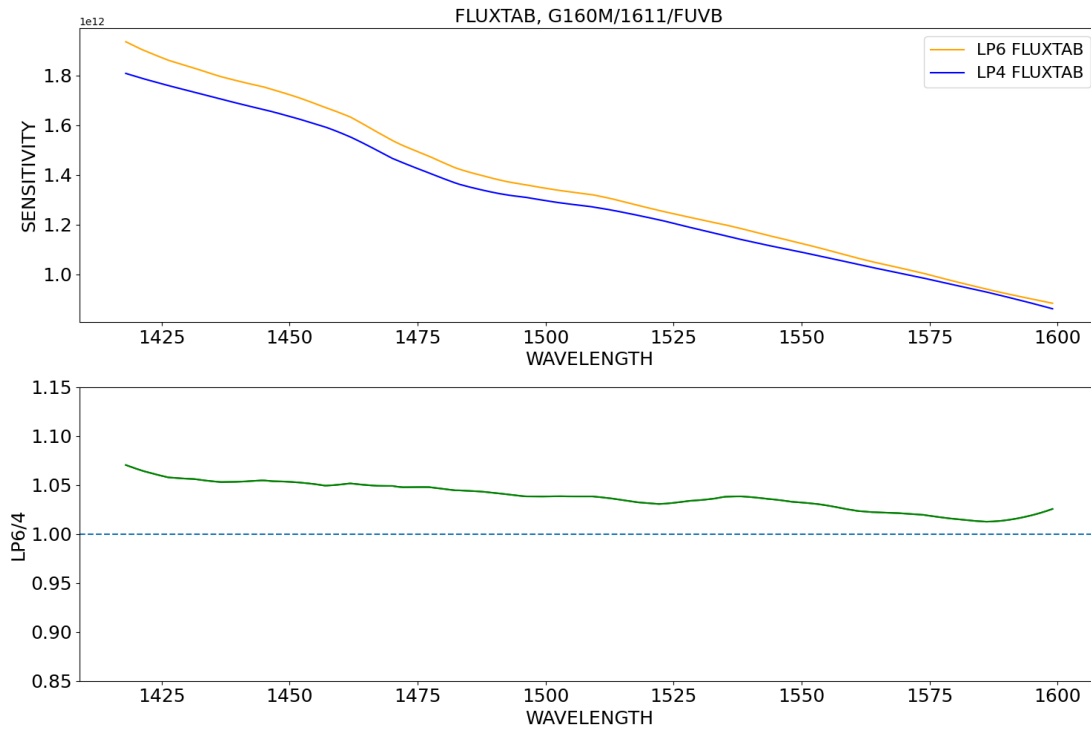


Figure A10.: The same as Fig. 3, but for G160M/1611/FUVB.

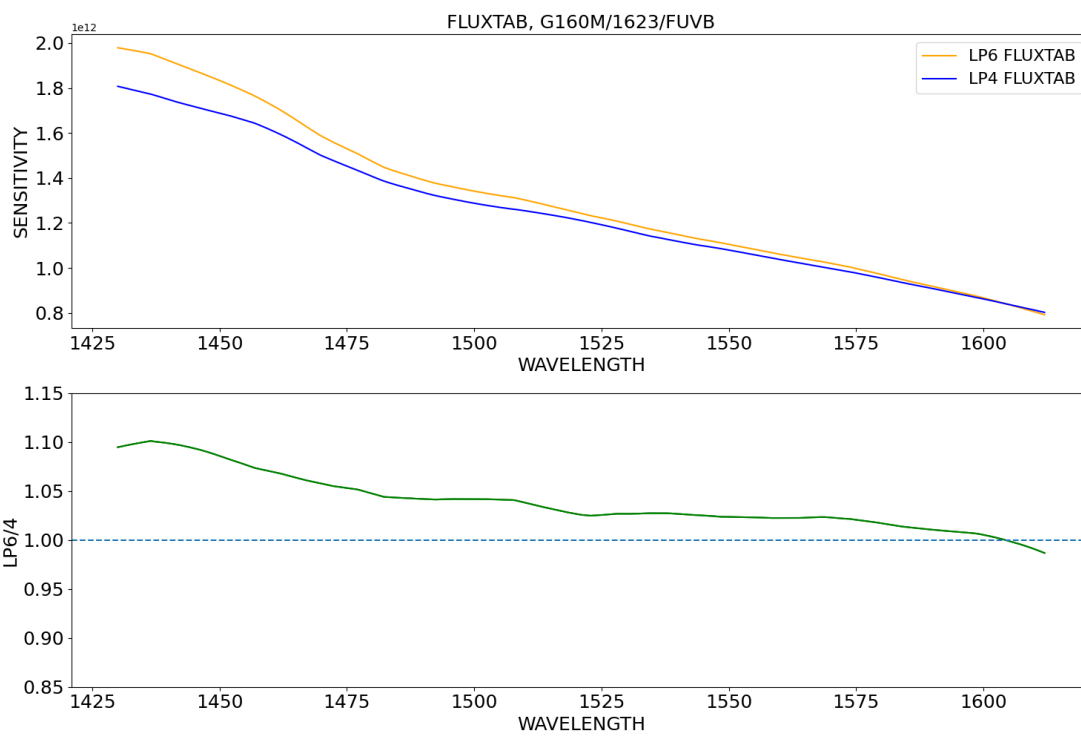


Figure A11.: The same as Fig. 3, but for G160M/1623/FUVB.

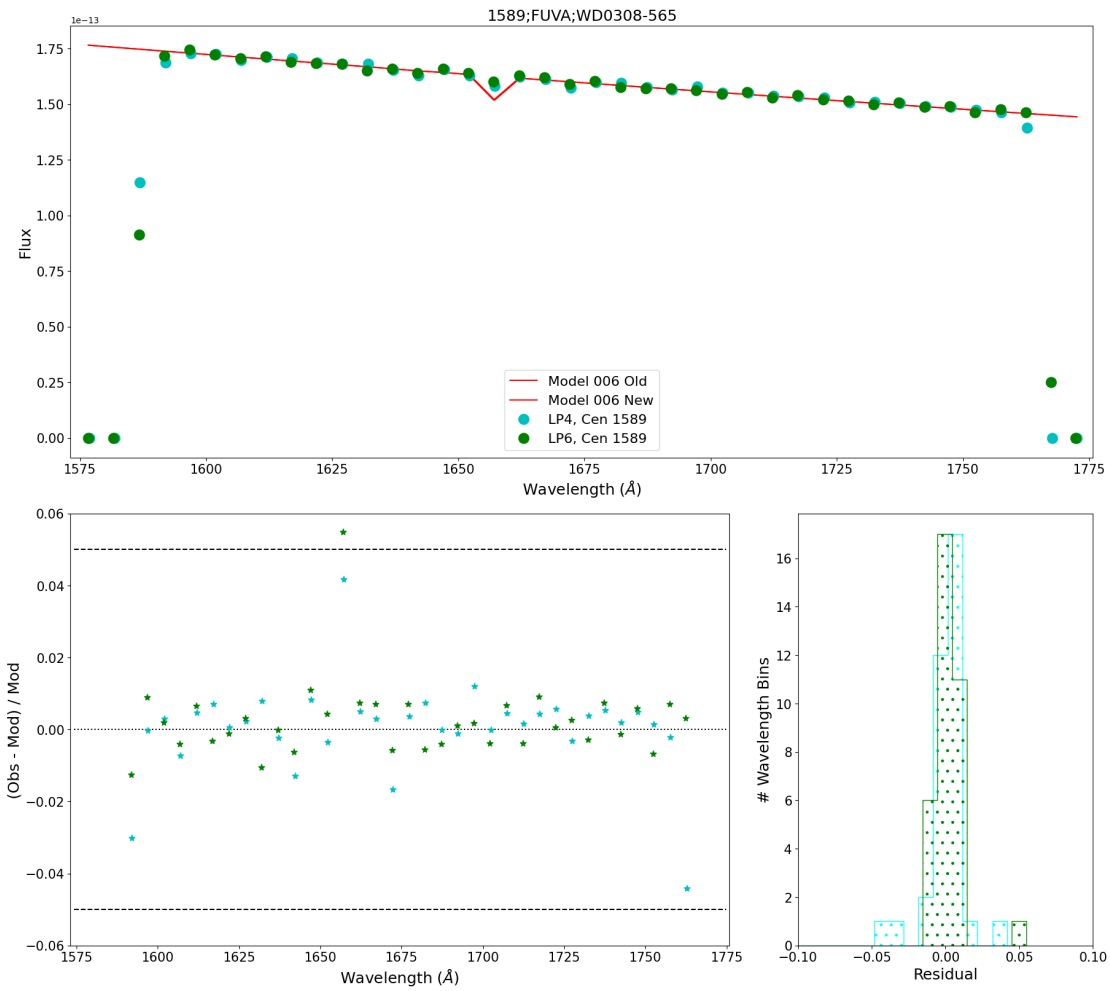


Figure A12.: The same as Fig. 6, but for G160M/1589/FUVA.

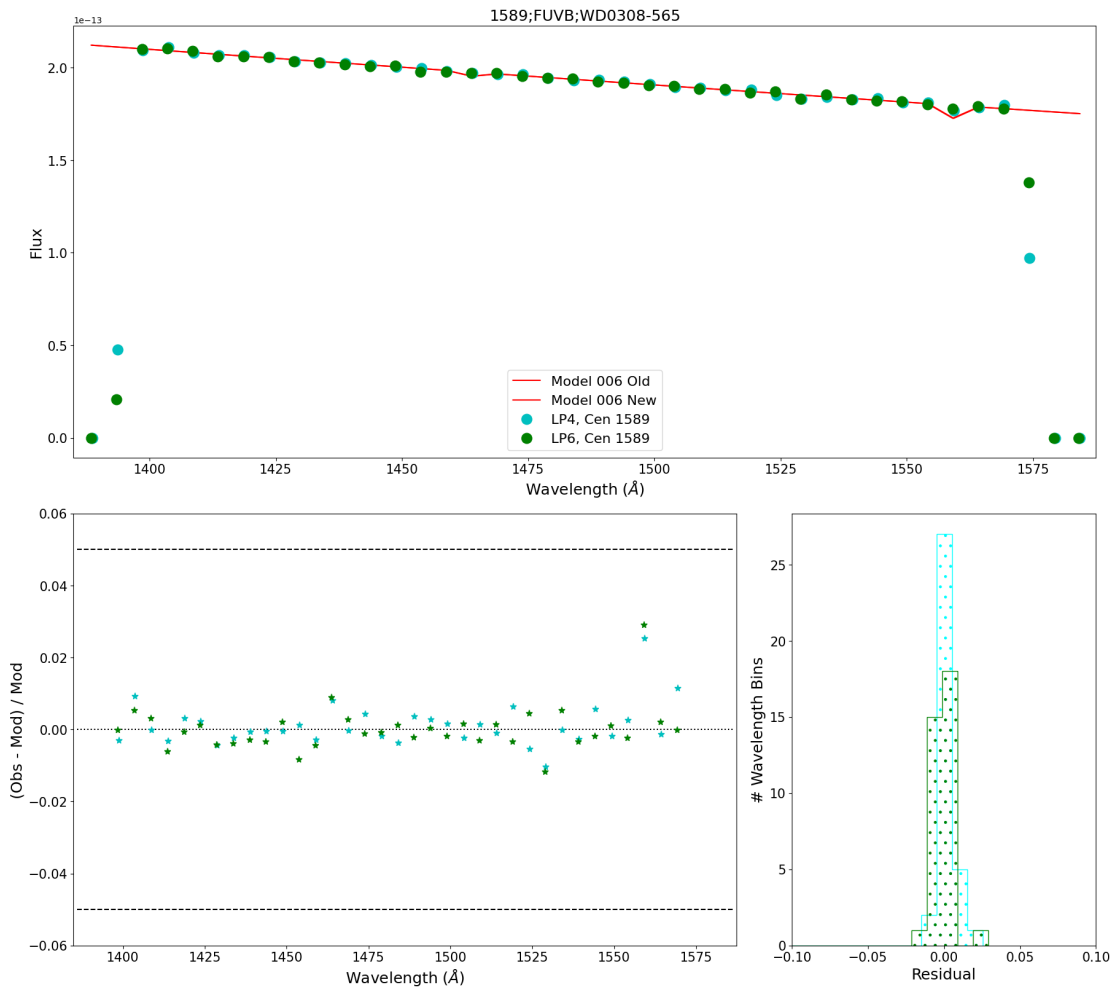


Figure A13.: The same as Fig. 6, but for G160M/1589/FUVB.

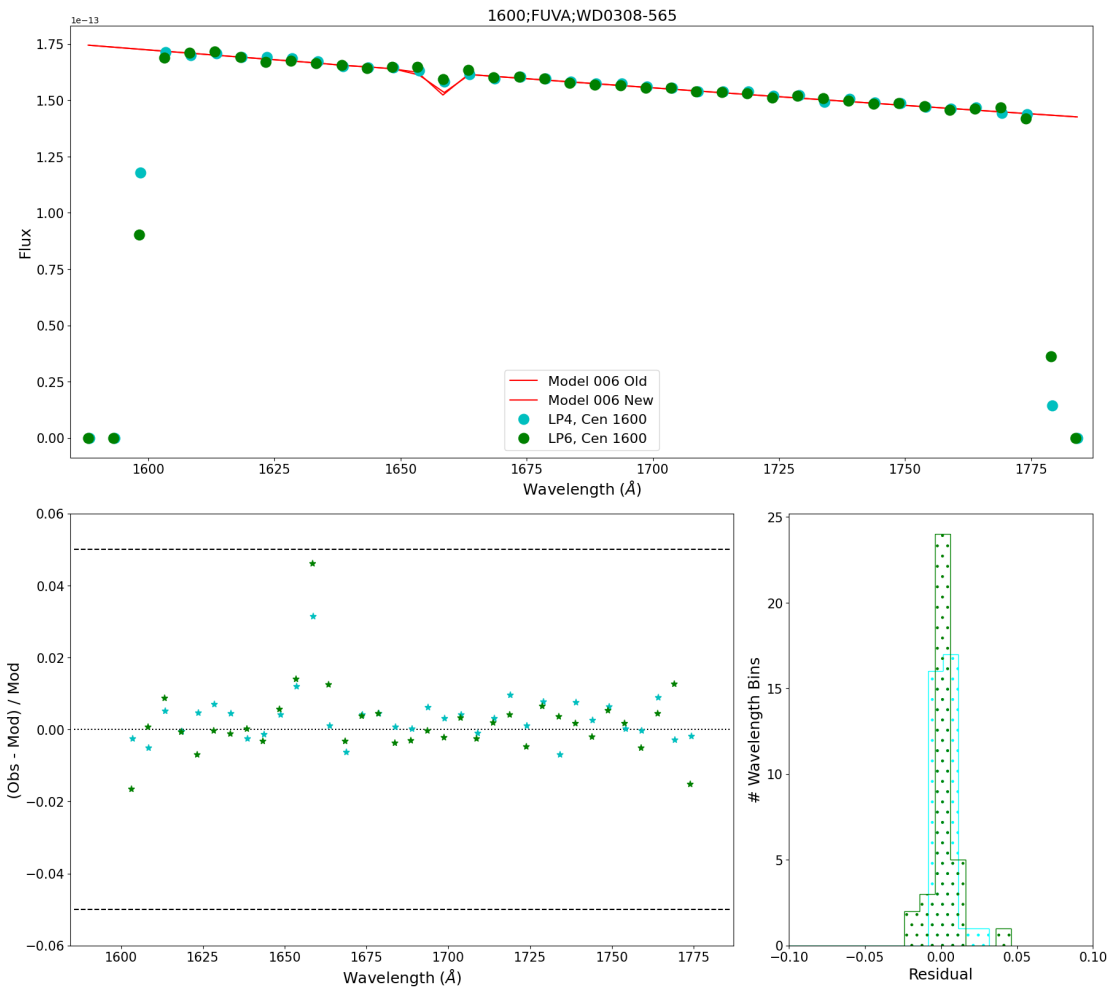


Figure A14.: The same as Fig. 6, but for G160M/1600/FUVA.

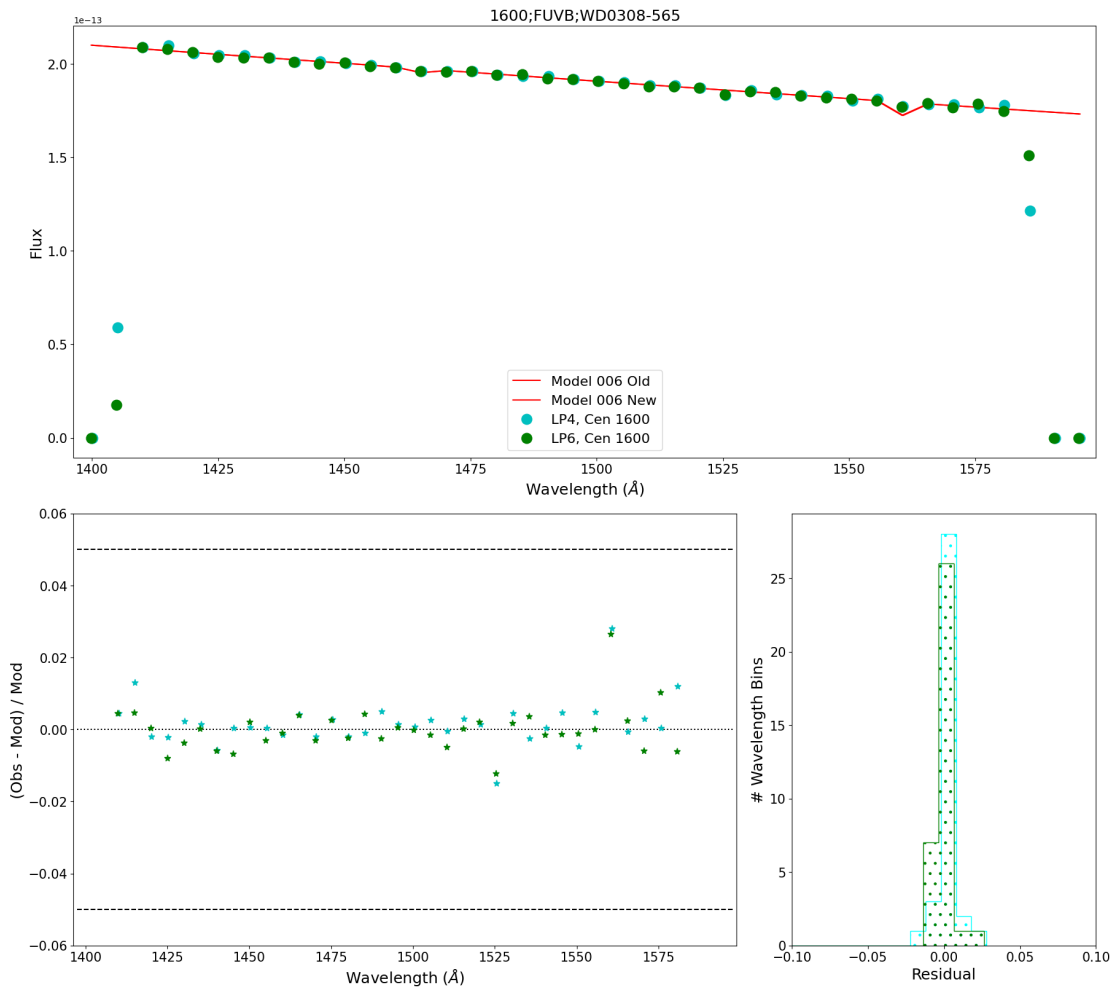


Figure A15.: The same as Fig. 6, but for G160M/1600/FUVB.

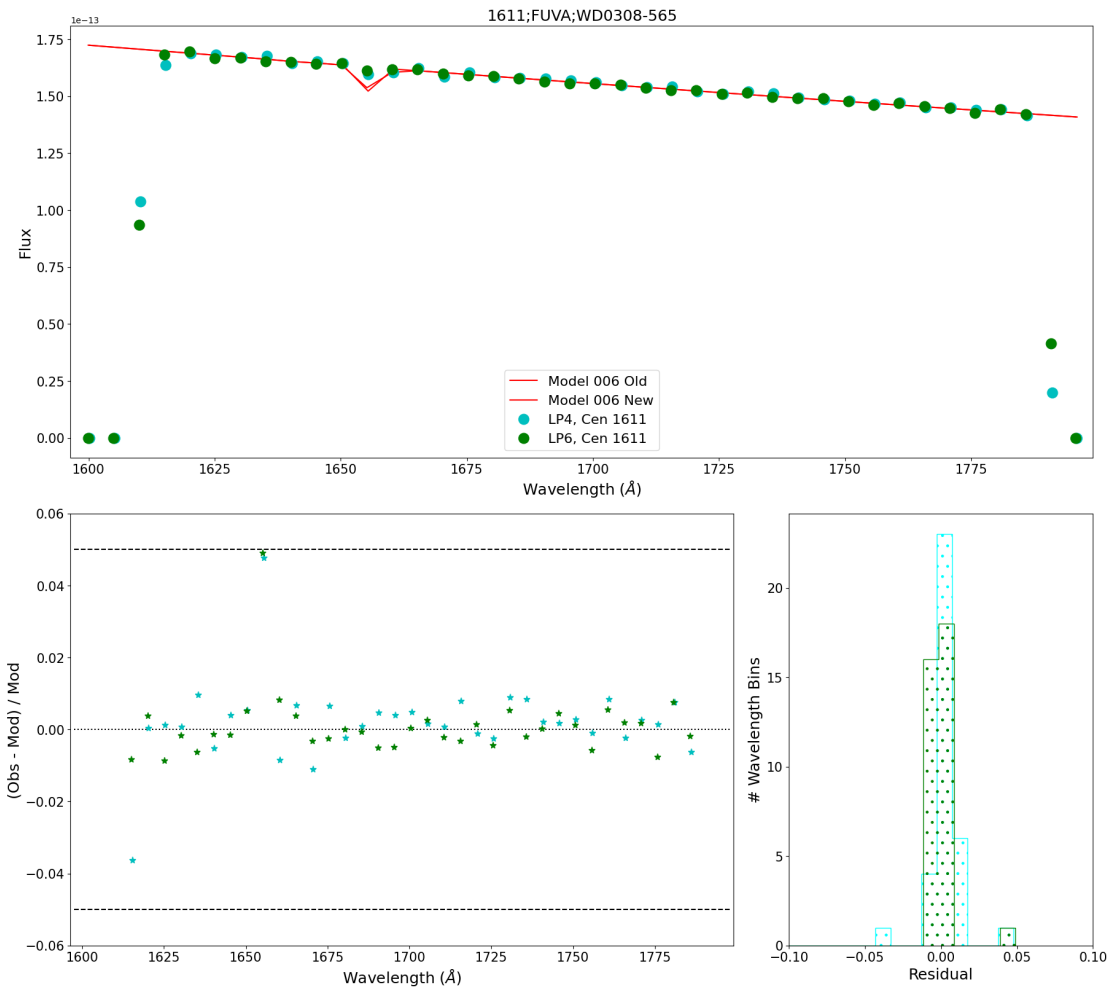


Figure A16.: The same as Fig. 6, but for G160M/1611/FUVA.

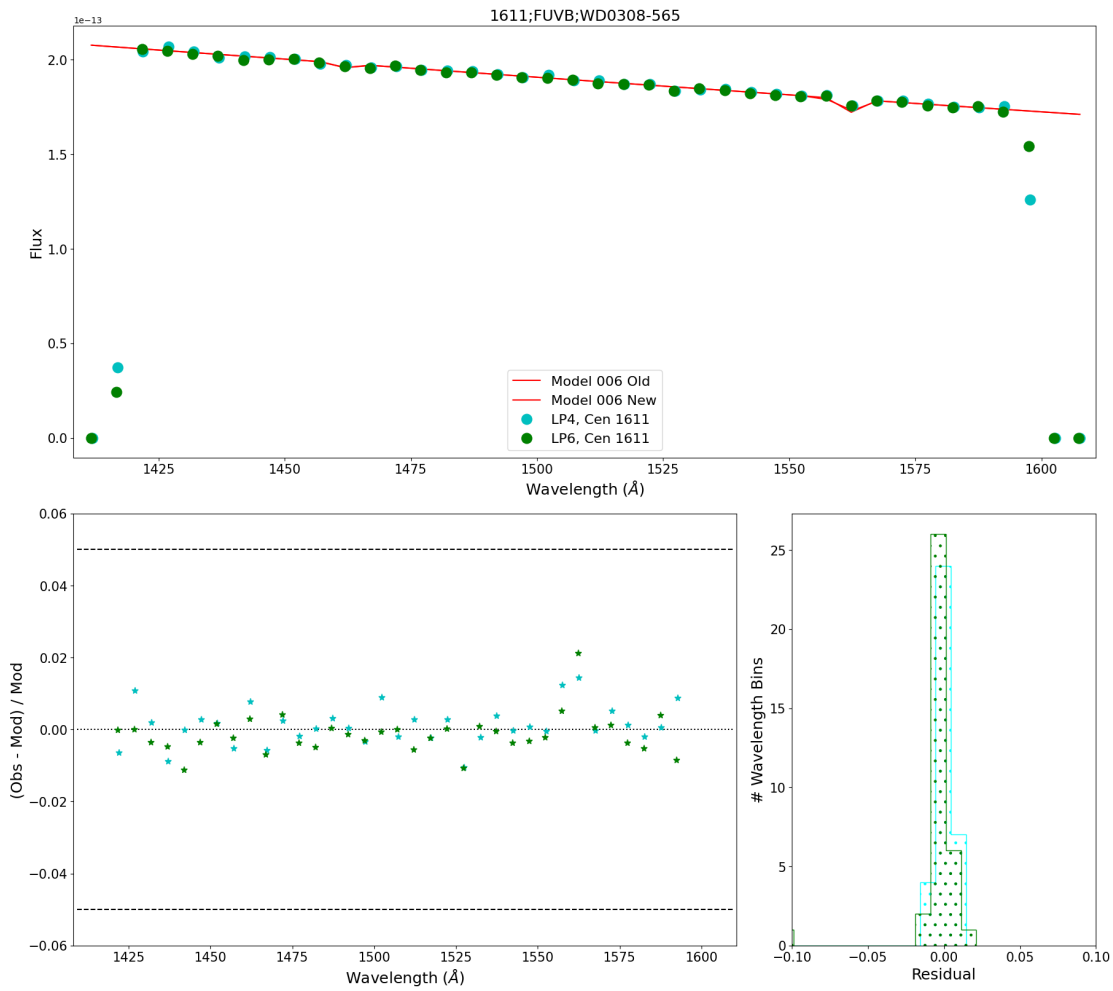


Figure A17.: The same as Fig. 6, but for G160M/1611/FUVB.

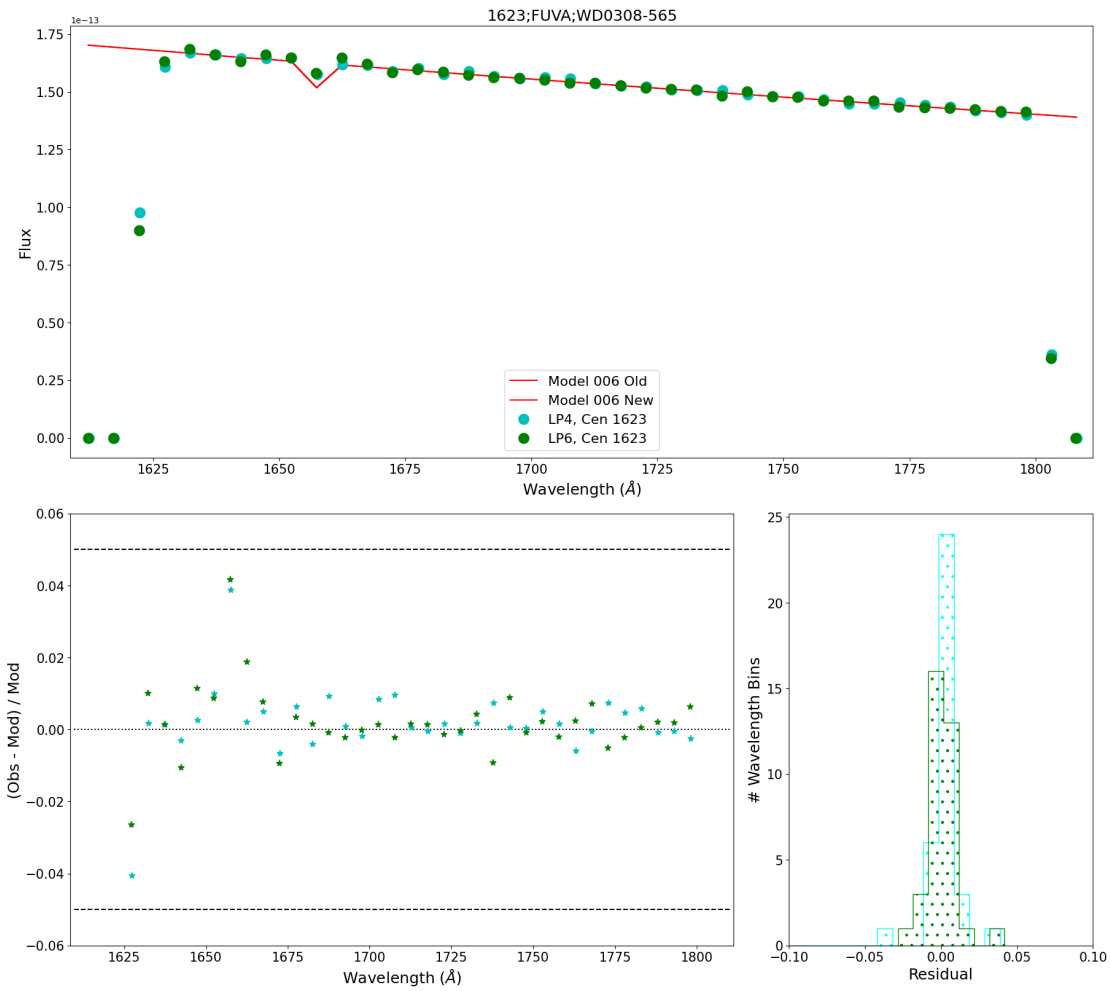


Figure A18.: The same as Fig. 6, but for G160M/1623/FUVA.

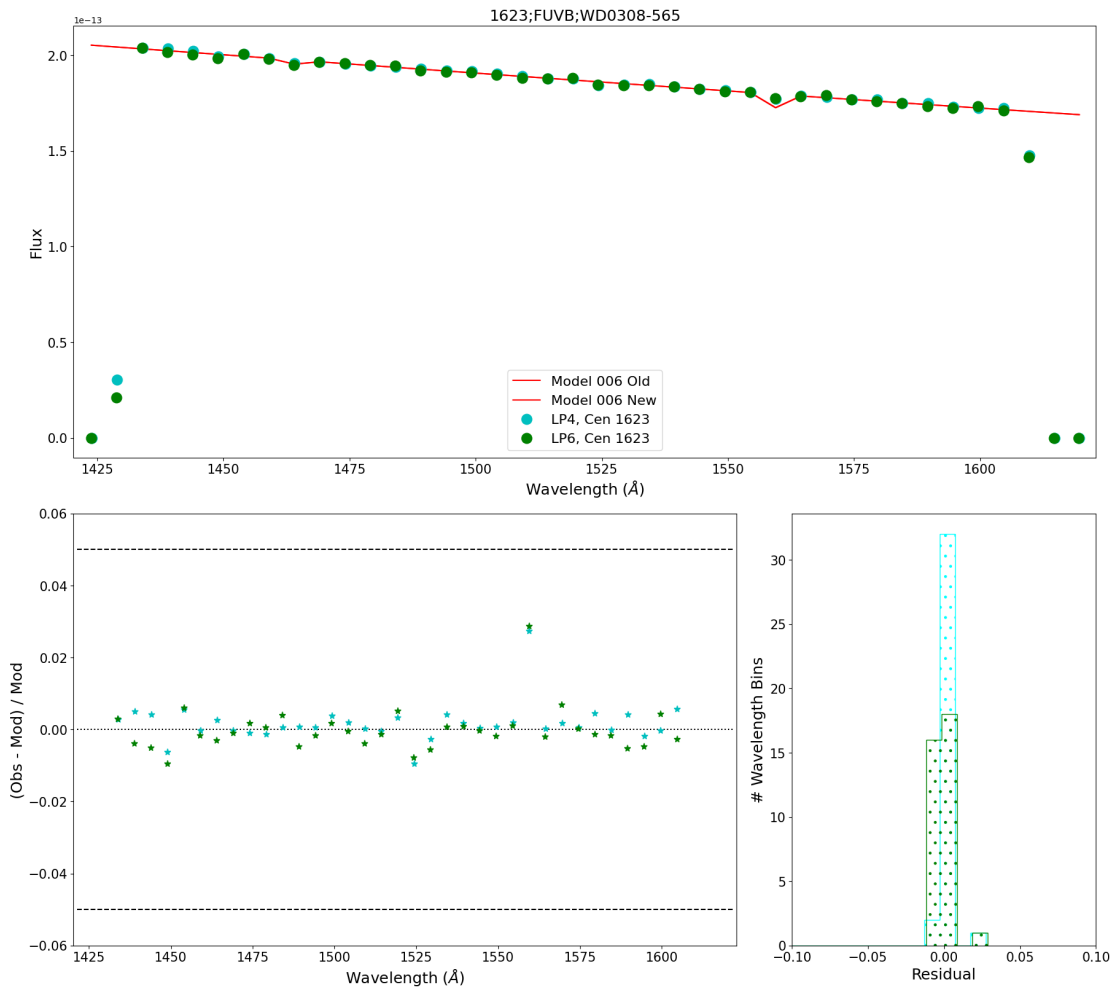


Figure A19.: The same as Fig. 6, but for G160M/1623/FUVB.